

DRAFT VERSION SEPTEMBER 25, 2025
 Typeset using **L^AT_EX preprint2** style in AASTeX7

Searching for GEMS: TOI-5349b is a Saturn-like planet orbiting a metal-rich early M-dwarf

ANGELI SANDOVAL ,¹ CALEB I. CAÑAS ,^{2,*} SHUBHAM KANODIA ,³ KNICOLE D. COLÓN ,²
 ANDREW MONSON ,⁴ ALEXANDER LARSEN ,⁵ TERA N. SWABY ,⁵ HENRY A. KOBULNICKY ,⁵
 PHILIP I. CHOI,⁶ SAGE SANTOMENNA ,⁶ PEI QIN,⁶ MICHAEL RODRUCK ,⁷
 WILLIAM D. COCHRAN ,⁸ NINA BROWN ,⁹ MADISON BRADY ,⁹ ANDREAS SEIFAHRT ,⁹
 ARVIND F. GUPTA ,¹⁰ JESUS HIGUERA ,¹⁰ MARK E. EVERETT ,¹⁰ ZURI BARKSDALE ,¹¹
 RITVIK BASANT ,⁹ JACOB L. BEAN ,⁹ SCOTT A. DIDDAMS ,^{12,13}
 GIANNINA GUZMÁN CALOCA ,^{14,2} SAMUEL HALVERSON ,¹⁵ JESSICA LIBBY-ROBERTS ,^{16,17}
 ANDREA S.J. LIN ,¹⁸ RAFAEL LUQUE ,^{9,19} ARPITA ROY ,²⁰ AND GUÐMUNDUR STEFÁNSSON ,²¹

¹*The Graduate Center of the City University of New York, 365 Fifth Avenue, New York, NY 10016, USA*

²*NASA Goddard Space Flight Center, 8800 Greenbelt Road, Greenbelt, MD 20771, USA*

³*Earth and Planets Laboratory, Carnegie Institution for Science, 5241 Broad Branch Road, NW, Washington, DC 20015, USA*

⁴*Steward Observatory, The University of Arizona, 933 N. Cherry Avenue, Tucson, AZ 85721, USA*

⁵*Department of Physics & Astronomy, University of Wyoming, Laramie, WY 82070, USA*

⁶*Pomona College, 333 N. College Way Claremont, CA 91711, USA*

⁷*Department of Physics, Engineering, and Astrophysics, Randolph-Macon College, Ashland, VA 23005, USA*

⁸*McDonald Observatory and Center for Planetary Systems Habitability, The University of Texas at Austin, Austin, TX 78730, USA*

⁹*Department of Astronomy & Astrophysics, University of Chicago, Chicago, IL 60637, USA*

¹⁰*U.S. National Science Foundation National Optical-Infrared Astronomy Research Laboratory, 950 N. Cherry Ave., Tucson, AZ 85719, USA*

¹¹*Department of Physics and Astronomy, Howard University, Washington, DC 20059, USA*

¹²*Electrical, Computer & Energy Engineering, University of Colorado, 425 UCB, Boulder, CO 80309, USA*

¹³*Department of Physics, University of Colorado, 2000 Colorado Avenue, Boulder, CO 80309, USA*

¹⁴*Department of Astronomy, University of Maryland, College Park, MD 20742, USA*

¹⁵*Jet Propulsion Laboratory, California Institute of Technology, 4800 Oak Grove Drive, Pasadena, California 91109*

¹⁶*Department of Astronomy & Astrophysics, 525 Davey Laboratory, The Pennsylvania State University, University Park, PA 16802, USA*

¹⁷*Center for Exoplanets and Habitable Worlds, 525 Davey Laboratory, The Pennsylvania State University, University Park, PA 16802, USA*

¹⁸*Department of Astronomy, California Institute of Technology, 1200 E California Blvd, Pasadena, CA 91125, USA*

¹⁹*NHFP Sagan Fellow*

²⁰*Astrophysics & Space Institute, Schmidt Sciences, New York, NY 10011, USA*

²¹*Anton Pannekoek Institute for Astronomy, University of Amsterdam, Science Park 904, 1098 XH Amsterdam, The Netherlands*

ABSTRACT

Corresponding author: Angeli Sandoval
 angelis0821@gmail.com

We report the confirmation and analysis of TOI-5349b, a transiting, warm, Saturn-like planet orbiting an early M-dwarf with a period of ~ 3.3 days, which we confirmed as part of the *Searching for GEMS* (Giant Exoplanets around M-dwarf Stars) survey. TOI-5349b was initially identified in photometry from NASA’s *Transiting Exoplanet Survey Satellite* (TESS) mission and subsequently confirmed using high-precision radial velocity (RV) measurements from the Habitable-zone Planet Finder (HPF) and MAROON-X spectrographs, and from ground-based transit observations obtained using the 0.6-m telescope at Red Buttes Observatory (RBO) and the 1.0-m telescope at the Table Mountain Facility of Pomona College. From a joint fit of the RV and photometric data, we determine the planet’s mass and radius to be $0.40 \pm 0.02 M_J$ ($127.4^{+5.9}_{-5.7} M_\oplus$) and $0.91 \pm 0.02 R_J$ ($10.2 \pm 0.3 R_\oplus$), respectively, resulting in a bulk density of $\rho_p = 0.66 \pm 0.06 \text{ g cm}^{-3}$ (~ 0.96 the density of Saturn). We determine that the host star is a metal-rich M1-type dwarf with a mass and radius of $0.61 \pm 0.02 M_\odot$ and $0.58 \pm 0.01 R_\odot$, and an effective temperature of $T_{\text{eff}} = 3751 \pm 59$ K. Our analysis highlights an emerging pattern, exemplified by TOI-5349, in which transiting GEMS often have Saturn-like masses and densities and orbit metal-rich stars. With the growing sample of GEMS planets, comparative studies of short-period gas giants orbiting M-dwarfs and Sun-like stars are needed to investigate how metallicity and disk conditions shape the formation and properties of these planets.

1. INTRODUCTION

Since its launch in 2018, NASA’s *Transiting Exoplanet Survey Satellite* (TESS; [G. R. Ricker et al. 2015](#)) has enabled the discovery of a wide range of exoplanets, including tens of giant planets around M-dwarfs so far, greatly expanding the previous population of these systems. These Giant Exoplanets around M-dwarf Stars (GEMS), which are typically defined by host stars with effective temperatures $T_{\text{eff}} \lesssim 4000$ K, and radii $8 R_\oplus \leq R_p \lesssim 15 R_\oplus$ or for the non-transiting ones, minimum masses $M_p \sin i \gtrsim 80 M_\oplus$ ([S. Kanodia et al. 2024a](#)). The *Searching for GEMS* survey ([S. Kanodia et al. 2024b](#)) is designed to explore the formation pathways of these gas giants around M-dwarfs by constraining their system properties, orbital architectures, and comparing them with similar systems.

GEMS are of particular interest because the presence of massive gas giants in low-mass stel-

lar environments challenges traditional planet formation models for core accretion. The prediction from theory is that gas giants are less likely to form *in-situ* (at their observed location) around low-mass stars due to reduced disk masses and longer core growth timescales ([G. Laughlin et al. 2004](#)). Observations of planets orbiting FGK dwarfs ([D. N. C. Lin et al. 1996](#)) and M-dwarfs (e.g., [S. Kanodia et al. 2023a](#); [M. J. Hobson et al. 2023](#); [A. P. Boss & S. Kanodia 2023](#)) propose that these planets formed at larger orbital separations through core accretion or gravitational instability and later migrated inward to their current orbits.

As part of the GEMS survey, we present the confirmation and characterization of TOI-5349b, a Saturn-like planet ($M_p = 0.40 M_J$, $R_p = 0.91 R_J$, $\rho_p = 0.66 \text{ g cm}^{-3}$) orbiting an early M-dwarf. We confirm the planetary nature of TOI-5349b using TESS photometry, ground-based photometry from the Red Buttes Observatory and the Table Mountain Facility of Pomona College, as well as high-precision radial

* NASA Postdoctoral Fellow

velocities (RVs) from the Habitable-zone Planet Finder (HPF) and MAROON-X spectrographs. In Section 2, we describe in more detail the photometric and radial velocity observations. In Section 3, we detail the characterization of the host star. Section 4 presents the joint modeling of the RV and photometric data. We discuss the implications of TOI-5349b in the context of the GEMS sample in Section 5, and summarize our conclusions in Section 6.

2. OBSERVATIONS

2.1. Photometry

2.1.1. TESS

TOI-5349.01 was first identified as a candidate using photometric observations from TESS as part of the faint star search for planet candidates around stars with TESS magnitude $T > 12$ (M. Kunimoto et al. 2022). The NASA TESS mission (G. R. Ricker et al. 2015) first observed TOI-5349 (TIC 26054627; Gaia DR3 58372904816938240) in Sector 42 (2021 August 20 – 2021 September 16), 43 (2021 September 16–2021 October 12) and 44 (2021 October 12–2021 November 6) at a 600 s cadence. The target was re-observed in Sectors 70 (2023 September 20 - 2023 October 16) and 71 (2023 October 16 – 2023 November 11) at a 200 s cadence. Similar to S. Kanodia et al. (2024a), we extracted the light curves from the TESS full-frame images (FFIs) for each sector using the TESS-Gaia Light Curve (`tglc`²²) pipeline (T. Han & T. D. Brandt 2023), which uses photometry from Gaia DR3 as priors to remove contamination from background stars. We used a 90×90 pixel cutout centered on TOI-5349 to sample the point-spread function and derive the contamination-corrected light curves. In this work, we analyzed the calibrated aperture light curves (`cal_aper_flux`) that are derived using

a 3×3 aperture centered on TOI-5349. The phase-folded photometry is shown in Figure 1.

2.1.2. Red Buttes Observatory 0.6-m telescope

We obtained two ground-based transit observations of TOI-5349 on 2023 January 4, and 2023 January 14, using the 0.6-m telescope at Red Buttes Observatory (D. H. Kasper et al. 2016) in Wyoming, USA. The transits were observed with the AltaF16 camera, employing a Bessel I filter and a plate scale of $0.731''/\text{pixel}$. Observations were performed with 2×2 on-chip pixel binning at a 240 s cadence. Weather and seeing conditions resulted in partial transits on both nights with RBO. The light curves of both visits were derived using differential photometry derived with `AstroImageJ` (K. A. Collins et al. 2017) in which we adopted an aperture radius of 7 pixels ($5.1''$), inner sky radius of 12 pixels ($8.8''$) and an outer sky radius of 17 pixels ($12.4''$). The RBO photometry is shown in Figure 2.

2.2. 1.0-m Table Mountain Facility of Pomona College

We also observed three transits (2025 January 3, 2025 January 14 and 2025 January 23) of TOI-5349 with Pomona College’s 1.0-m telescope located at NASA Jet Propulsion Laboratory’s Table Mountain Facility in California, USA. The visibility from Table Mountain only allowed for an observation of partial transits (mid-transit through egress) on 2025 3 January and 14 January. The telescope was operated with 1×1 binning, a gain of $0.8 \text{ e}^-/\text{ADU}$, and a plate scale of $0.232''/\text{pixel}$. All observations used a 10-second exposure time and were obtained in the Sloan i' filter. Light curves for all visits were extracted using `AstroImageJ`, using an aperture radius of 17 pixels ($3.9''$), an inner sky radius of 29 pixels ($6.7''$), and an outer sky radius of 44 pixels ($10.2''$). The Pomona photometry is shown in Figure 2.

²² https://github.com/TeHanHunter/TESS_Gaia_Light_Curve

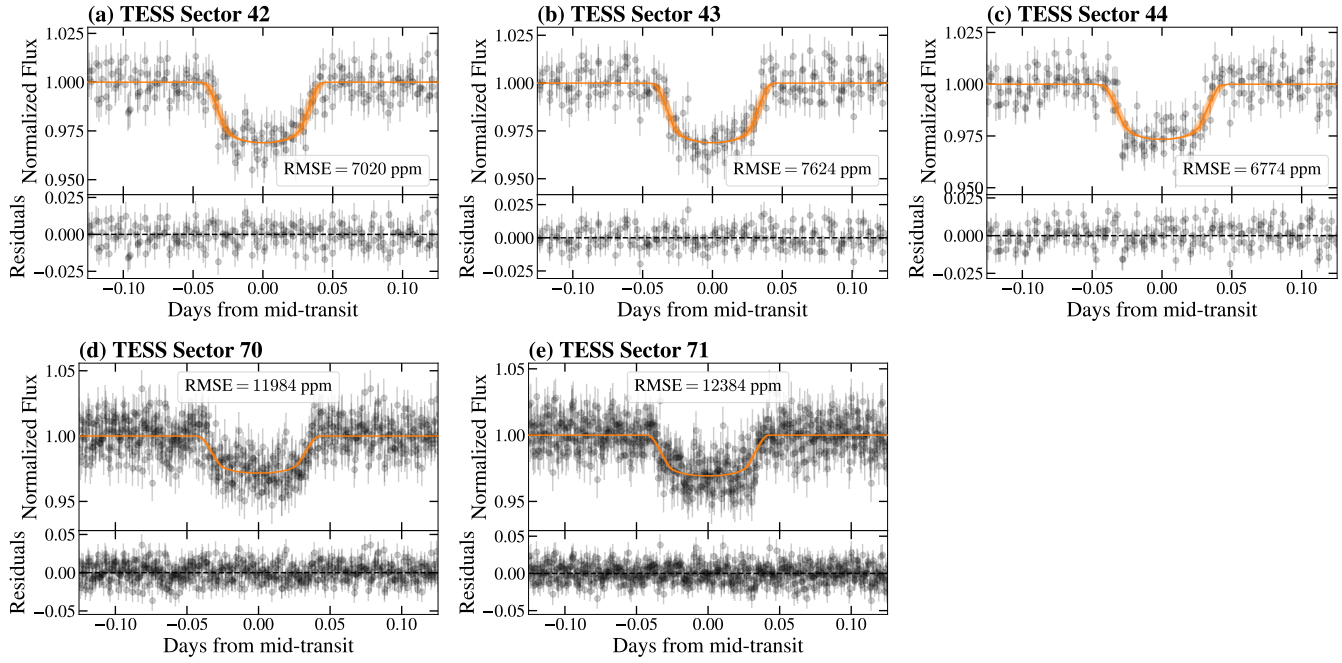


Figure 1. (a)-(e) Median normalized, phase-folded TESS light curves for various sectors of TOI-5349 derived with `tglc`. The solid line is the best-fitting transit model. In each panel, the shaded regions are the 1σ (darkest), 2σ , and 3σ (lightest) extent of the model posteriors. The root mean square error (RMSE) is indicated for reference. See Section 4 for a detailed description of the modeling.

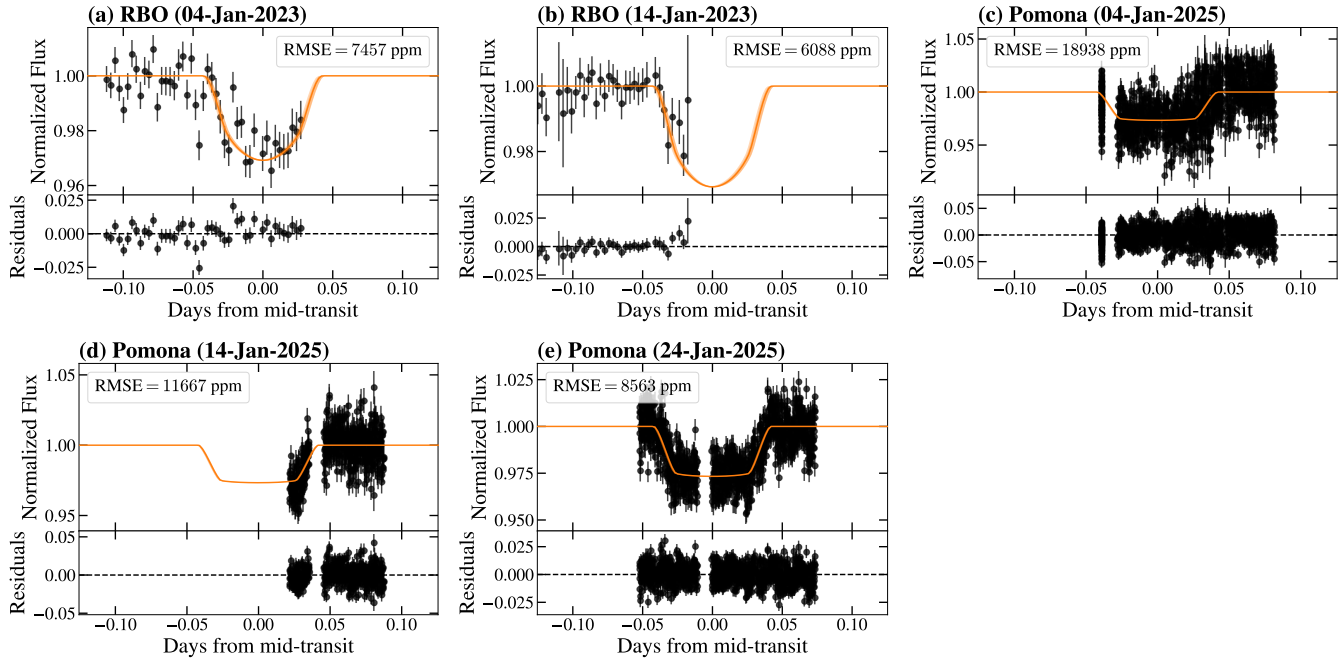


Figure 2. (a)-(e) Identical to Figure 1 but for ground-based RBO (Bessel I) and Pomona (Sloan i') data.

2.3. High-resolution spectroscopy

2.3.1. HPF

Between 2022 October 22 – 2024 January 29, we obtained 13 visits of TOI-5349 with the

Habitable-zone Planet Finder (HPF), a high-resolution, near-infrared ($8080 - 12780 \text{ \AA}$) spectrograph ($R \sim 55,000$) that is installed on the 10-m Hobby-Eberly Telescope located at the

McDonald Observatory in Texas, USA (L. W. Ramsey et al. 1998; G. J. Hill et al. 2021). HPF is a fiber-fed (S. Kanodia et al. 2018), thermally stabilized (G. Stefansson et al. 2016), spectrometer that was designed to obtain high-precision RVs in the near-infrared (S. Mahadevan et al. 2012, 2014). Each visit consisted of two exposures of 945 seconds each and were executed in a queue operated by HET resident astronomers (M. Shetrone et al. 2007). The raw spectral data are processed using the `HXRGproc`²³ package following the methods described in J. P. Ninan et al. (2018). We performed barycentric correction utilizing the `barycorppy`²⁴ package (S. Kanodia & J. Wright 2018) developed from the algorithms in J. T. Wright & J. D. Eastman (2014). The RV measurements for each 945 s exposure are then derived from the spectra using HPF-SERVAL²⁵ (G. Stefánsson et al. 2023), a modified version of the template matching `SpEctrum Radial Velocity AnaLyser` (SERVAL) framework (M. Zechmeister et al. 2018). The HPF data have a median per-pixel signal-to-noise (S/N) per unbinned exposure (of 945 s) at 1070 nm of 32. The binned RVs (weighted average of the two exposures) and the respective uncertainties are listed in Table 1 and shown in Figure 3.

2.3.2. MAROON-X

We obtained six visits of TOI-5349 between 2023 October 14 and October 28 (Program GN-2023B-Q-104, PI Kanodia) using MAROON-X, a high-resolution ($R \sim 85,000$), red-optical spectrograph on the 8.1-m Gemini North telescope (A. Seifahrt et al. 2016, 2018, 2020, 2022). MAROON-X has two channels with different wavelength coverage consisting of a “blue” channel that spans 5000 – 6700 Å and a “red” channel that covers 6500 – 9000 Å.

²³ <https://github.com/indiajoe/HxRGproc>

²⁴ <https://github.com/shbhuk/barycorppy>

²⁵ https://github.com/gummikis/hpfserval_lhs3154.git

All visits used a fixed exposure time of 1800 s, which provided a median peak S/N of 28.5 and 51.5 in the blue and red channels, respectively. Both channels were exposed simultaneously during each visit. We reduced the data using a custom pipeline originally developed for the CRIRES instrument as outlined in (J. L. Bean et al. 2010) and measured the RVs for each channel using a modified version of the SERVAL algorithm (M. Zechmeister et al. 2018). The derived RVs and the respective uncertainties for each channel are listed in Table 1 and shown in Figure 3. Each channel is considered a separate instrument when fitting the data (see Section 4 for details).

2.4. Excluding an eclipsing binary scenario with spectroscopy

We note that since our photometry does not include multiple band passes to vet our object for eclipsing binaries, we relied on high-resolution spectroscopy to exclude this possibility. Our RV time series with HPF began prior to any ground-based transit observations, allowing us to test for stellar companions at the transit period. The HPF RV data did not show evidence of large-amplitude variations or secondary star light that would signify a binary. We further examined the differential line width and the chromatic RV index calculated by HPF-SERVAL which are proxies for line deformations that may be due to binarity or stellar activity (see §4 in M. Zechmeister et al. 2018). These HPF-SERVAL diagnostics displayed no significant variations or correlations with our observed RVs, suggesting that there were no significant line profile distortions in our HPF spectra.

Subsequent MAROON-X observations, obtained at a higher signal-to-noise ratio, confirmed these findings, where the measured RV signal was consistent with a planetary companion and not a binary signal and the MAROON-X differential line width values likewise showed no correlation with the RV data. We there-

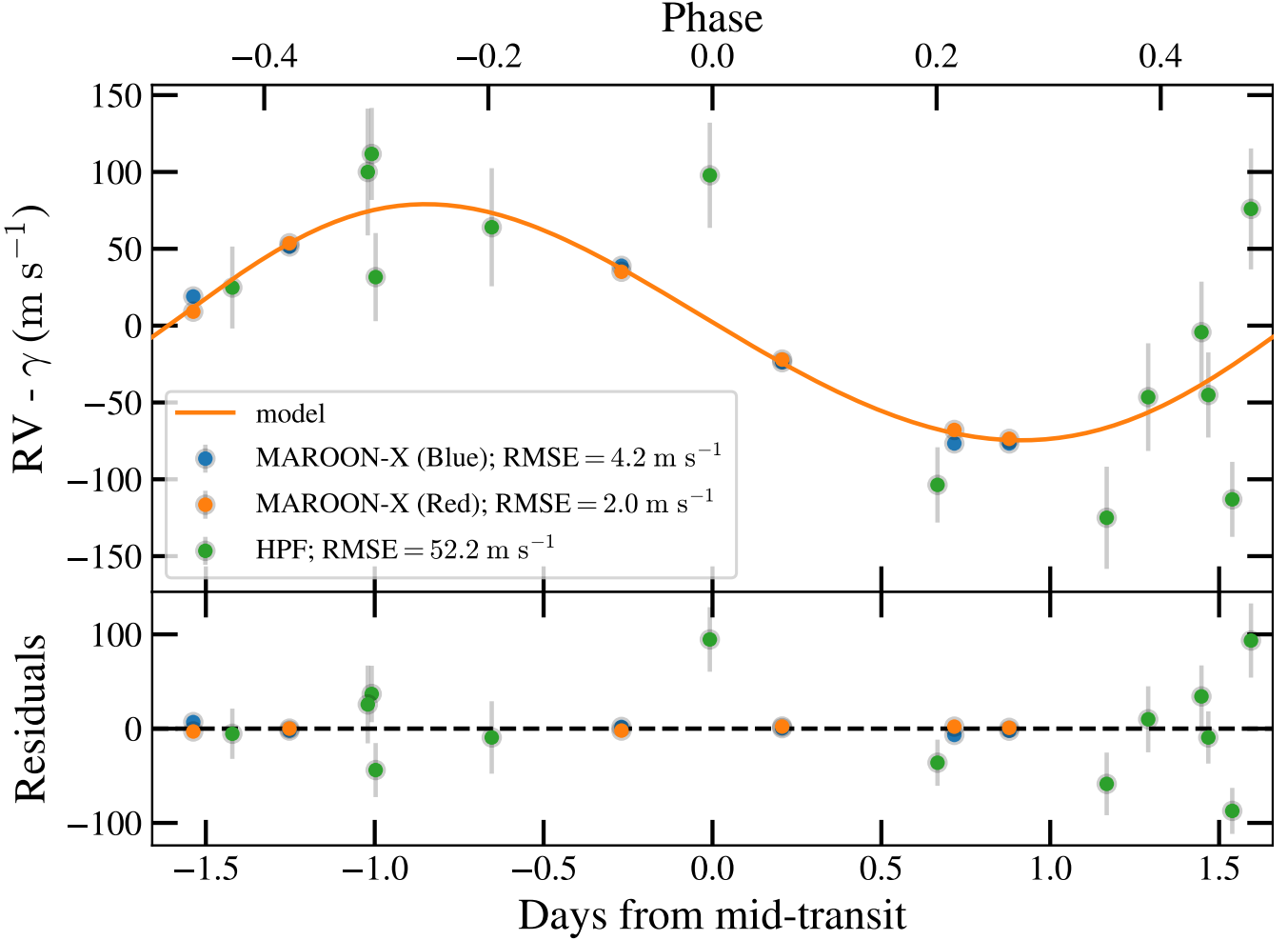


Figure 3. **Top:** Phase-folded RVs for TOI-5349 derived with **SERVAL**. The best-fitting Keplerian model is denoted with a solid line. The shaded regions denote the 1 σ (darkest), 2 σ , and 3 σ (lightest) extent of the model posteriors. The uncertainties for MAROON-X are too small to visualize at the scale shown. **Bottom:** Phase-folded residuals to the fit. The modeling is described in Section 4.

fore conclude that these spectroscopic diagnostics exclude the possibility of an eclipsing binary in the confirmation of TOI-5349b. Furthermore, after we modeled the photometry and RVs (Section section 4), we confirmed that our measured stellar density was identical to the density derived from the transit (within 1 σ ; see S. Seager & G. Mallén-Ornelas 2003; J. N. Winn 2010; D. M. Kipping 2014) which suggested TOI-5349b was indeed a planet orbiting this M-dwarf.

2.5. Speckle imaging with NESSI

We observed TOI-5349 on the night of 2022 September 18 using the NN-Explore Exoplanet

Stellar Speckle Imager (NESSI; N. J. Scott et al. 2018), a dual-channel speckle imager on the WIYN 3.5-m Telescope at Kitt Peak National Observatory (PI Gupta, 2022B-936991). TOI-5349 was observed in both the Sloan g' and i' filters and the images were reconstructed following the procedures described in S. B. Howell et al. (2011). Figure 5 presents the 5 σ contrast curves, which reveal that there are no bright ($\Delta i' < 3.5$ and $\Delta g' < 4.0$) companions at separations of 0.15 – 1.2 $''$ from TOI-5349. To assess whether TOI-5349 is part of a wide-separation binary system, we cross-matched it with the K. El-Badry et al. (2021); K. El-Badry (2021) cata-

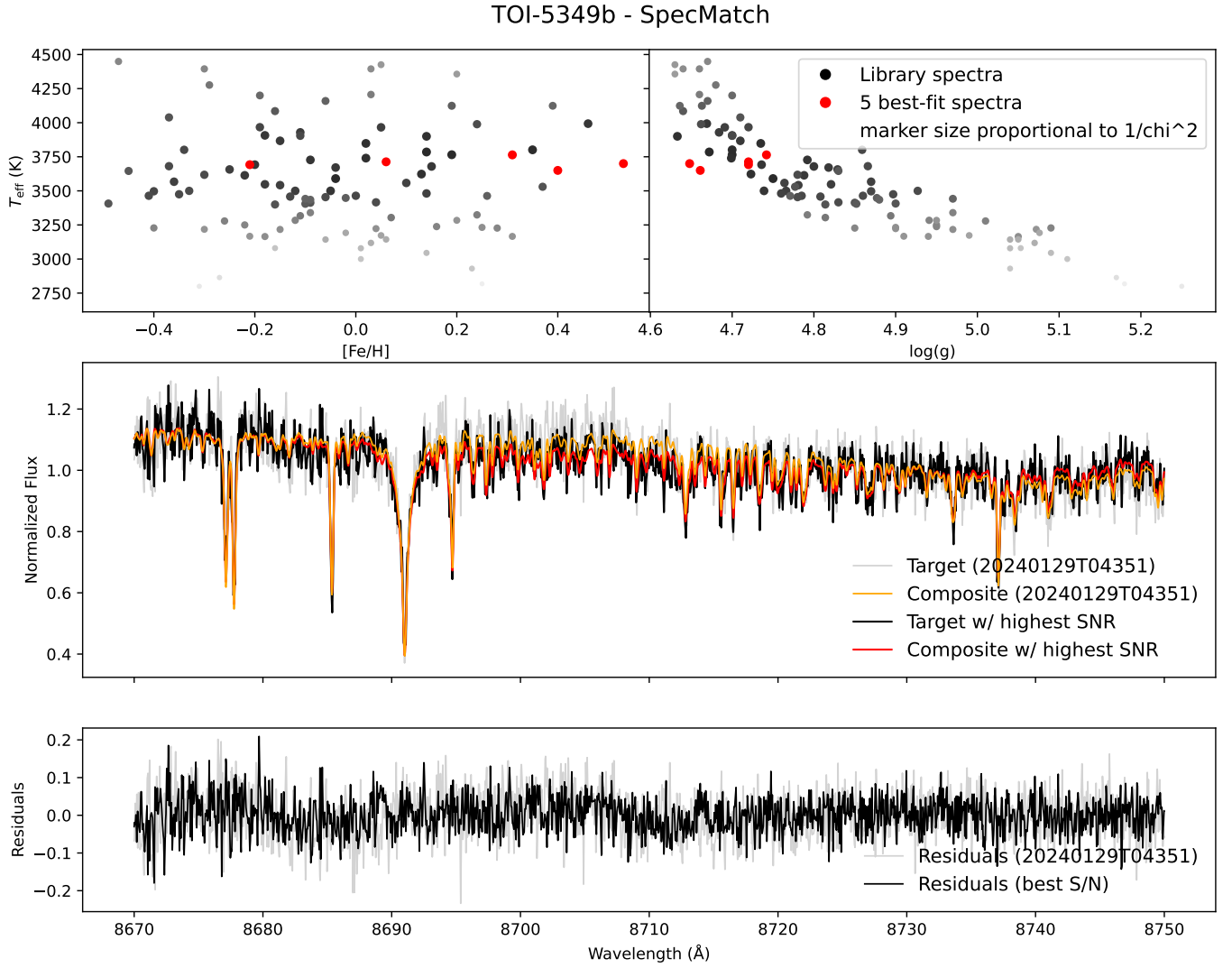


Figure 4. TOI-5349’s HPF–SpecMatch spectral fit results for order index 5. Top: two panels show the five best-fit library stars in red that were selected to construct the composite spectrum of TOI-5349b. The size and shading of both the best-fit stars (red) and the remaining library stars (black) scale inversely with the initial χ^2 value, where larger and darker points represent better matches to the target spectrum. Middle: the HPF order 5 spectrum compared to its best-fit composite (orange). Bottom: residuals between the spectrum and best-fit composite (black).

\log^{26} and found that it is not listed as a resolved wide binary in Gaia DR3, consistent with the Speckle Imager results.

3. STELLAR CHARACTERIZATION

3.1. *Spectroscopic parameters with HPF*

We derived the stellar effective temperature (T_e), surface gravity ($\log g_*$), metallicity

($[\text{Fe}/\text{H}]$), and rotational broadening ($v \sin i_*$) from HPF spectra of TOI-5349 using the HPF-SpecMatch²⁷ package (G. Stefánsson et al. 2020). HPF-SpecMatch follows a similar methodology presented by S. W. Yee et al. (2017) to derive spectroscopic parameters using a weighted linear-combination of the five best-

²⁷ <https://gummiks.github.io/hfpspecmatch/>

²⁶ <https://zenodo.org/records/4435257>

Table 1. RVs for TOI-5349.

Time BJD _{TDB}	RV m s ⁻¹	σ m s ⁻¹	Instrument
2459874.965870	64.83	32.89	HPF
2459884.939955	23.96	27.70	HPF
2459897.910783	-55.94	33.24	HPF
2459915.642095	180.81	29.95	HPF
2459916.643227	166.92	34.24	HPF
2459922.633343	133.12	38.43	HPF
2459924.825907	-43.96	24.41	HPF
2459954.742606	145.06	39.35	HPF
2459967.709932	22.55	35.04	HPF
2459978.670997	169.07	41.28	HPF
2459988.648056	100.66	28.67	HPF
2460223.796071	93.89	26.66	HPF
2460338.693217	-34.54	24.50	HPF
2460232.059785	-5.09	3.87	MAROON-X (Blue)
2460234.901990	57.58	4.72	MAROON-X (Blue)
2460235.887519	-57.93	4.78	MAROON-X (Blue)
2460236.952051	37.69	3.67	MAROON-X (Blue)
2460243.872681	70.20	4.93	MAROON-X (Blue)
2460246.003767	-57.95	3.36	MAROON-X (Blue)
2460232.059785	-3.33	3.22	MAROON-X (Red)
2460234.901990	53.81	3.84	MAROON-X (Red)
2460235.887519	-49.14	3.91	MAROON-X (Red)
2460236.952051	27.83	3.03	MAROON-X (Red)
2460243.872681	72.33	3.96	MAROON-X (Red)
2460246.003767	-54.91	2.72	MAROON-X (Red)

NOTE—The reported HPF RVs are the weighted average of the RVs for measured from the individual 945s exposure.

matching empirical spectra from a library of well-characterized stars. In this work, the HPF spectral library consisted of 100 stars that span $2700\text{K} \leq T_e \leq 4500\text{ K}$, $4.63 < \log g_\star < 5.26$, and $-0.49 < [\text{Fe}/\text{H}] < 0.53$. Spectral matching was performed using the region covering $8534 - 8645\text{ \AA}$ (HPF order index 5) due to minimal telluric contamination and the parameter

uncertainties were the standard deviation of the residuals from a leave-one-out cross-validation procedure applied to the library.

[Table 2](#) presents the derived spectroscopic parameters with their uncertainties. TOI-5349 is determined to have $T_e = 3751 \pm 59\text{ K}$, $\log g_\star = 4.72 \pm 0.05$, and $[\text{Fe}/\text{H}] = 0.50 \pm 0.16$. The resolution limit of HPF ($R \sim 55,000$) can only

Table 2. Summary of stellar parameters for TOI-5349.

Parameter	Description	Value	Reference
Main identifiers:			
TIC	TESS Input Catalog ID	26054627	TIC
TOI	TESS Object of Interest ID	5349	TSO
Gaia DR3	Gaia Source ID	58372904816938240	Gaia DR3
Coordinates, proper motion, distance, maximum extinction, and spectral type:			
α_{J2016}	Right Ascension (RA)	03:30:51.01	Gaia DR3
δ_{J2016}	Declination (Deg)	20:52:46.65	Gaia DR3
μ_{α}	Proper motion (RA, mas yr $^{-1}$)	37.20 ± 0.03	Gaia DR3
μ_{δ}	Proper motion (Dec, mas yr $^{-1}$)	-19.56 ± 0.02	Gaia DR3
l	Galactic longitude	165.83445	Gaia DR3
b	Galactic latitude	-28.41487	Gaia DR3
ϖ	Parallax (mas)	5.26 ± 0.03	Gaia DR3
$A_{V,\text{max}}$	Maximum visual extinction	0.04	Green
Spectral type	...	$M1 \pm 0.5$	LAMOST
Broadband photometric magnitudes:			
g'	PS1 g' mag	16.38 ± 0.01	PanSTARRS
r'	PS1 r' mag	15.155 ± 0.004	PanSTARRS
i'	PS1 i' mag	14.242 ± 0.001	PanSTARRS
z'	PS1 z' mag	13.84 ± 0.01	PanSTARRS
y'	PS1 y' mag	13.622 ± 0.008	PanSTARRS
T^a	TESS T mag	13.8117	TIC
J	2MASS J mag	12.43 ± 0.02	2MASS
H	2MASS H mag	11.73 ± 0.02	2MASS
K_s	2MASS K_s mag	11.51 ± 0.02	2MASS
W1	WISE1 mag	11.4 ± 0.2	WISE
W2	WISE2 mag	11.45 ± 0.02	WISE
W3	WISE3 mag	11.3 ± 0.2	WISE
Spectroscopic parameters from HPF-SpecMatch:			
T_e	Effective temperature (K)	3751 ± 59	This work
$\log g_{\star}$	Surface gravity (cgs)	4.72 ± 0.04	This work
[Fe/H]	Metallicity (dex)	0.50 ± 0.16	This work
$v \sin i_{\star}$	Rotational broadening (km s $^{-1}$)	< 2	This work
Model-dependent parameters from a stellar SED and isochrone fit b :			
M_{\star}	Mass (M_{\odot})	0.61 ± 0.02	This work
R_{\star}	Radius (R_{\odot})	0.58 ± 0.01	This work
L_{\star}	Luminosity (L_{\odot})	0.063 ± 0.002	This work
ρ_{\star}	Density (g cm $^{-3}$)	4.4 ± 0.3	This work
d	Distance (pc)	190 ± 1	This work
A_v	Visual extinction (mag)	0.02 ± 0.01	This work
Age	Age (Gyrs)	9^{+3}_{-4}	This work
Other stellar parameters:			
RV	Systemic RV (km s $^{-1}$)	40.42 ± 0.05	This work
$(U, V, W)_{\text{LSR}}$	Galactic velocities w.r.t. LSR c (km s $^{-1}$)	$-36.2 \pm 0.8, -13.9 \pm 0.5, -4.7 \pm 0.4$	This work

References—TIC (K. G. Stassun et al. 2019), TSO (N. M. Guerrero et al. 2021), Gaia DR3 (Gaia Collaboration et al. 2022), Green (G. M. Green et al. 2019), LAMOST (J. Zhong et al. 2019), PanSTARRS (K. C. Chambers et al. 2016), 2MASS (R. M. Cutri et al. 2003), WISE (E. L. Wright et al. 2010)

a TESS is not used in the SED fit.

b Derived with the EXOFastv2 package using MIST isochrones.

c Calculated using the solar velocities from R. Schönrich et al. (2010).

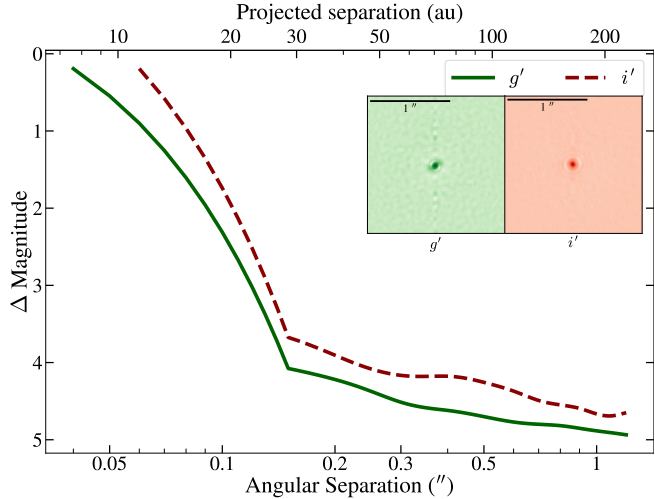


Figure 5. The 5σ contrast curves for TOI-5349 obtained with NESSI. The data reveal no bright companions at separations of $0.15'' - 1.2''$. The insets are the reconstructed images centered on TOI-5349 in the Sloan g' and Sloan i' filters.

place an upper limit of $v \sin i < 2 \text{ km s}^{-1}$. Similar to the previous results from the *Searching for GEMS* survey (L. M. Bernabò et al. 2024; S. Kanodia et al. 2024a; V. Reji et al. 2025), we note that the complexities of M-dwarf spectra and limitations in the HPF-SpecMatch algorithm limit the accuracy of the derived metallicity. We advise caution in interpreting the [Fe/H] beyond a qualitative indicator that TOI-5349 is super-solar in metallicity, especially as it is near the edge of the existing library.

3.2. Stellar classification from LAMOST

The Large Sky Area Multi-Object Fibre Spectroscopic Telescope (LAMOST) is a 4-m telescope that uses 4000 fibers distributed over a 5° field of view to acquire low-resolution ($R \approx 1800$) spectra in the optical (3700-9000Å) band (X.-Q. Cui et al. 2012). TOI-5349 was observed on 27 December 2015 as part of a spectroscopic survey of the Galactic anticenter (L.-C. Deng et al. 2012; H. B. Yuan et al. 2015; M. S. Xiang

et al. 2017) and the spectrum was made public as part of DR10v2.0²⁸ (X.-Y. Wang et al. 2022).

LAMOST DR10 derives a spectral type, spectroscopic parameters and uncertainties (derived via cross-validation) using an empirical sample of 1365 high S/N M-dwarfs (B. Du et al. 2021, 2024). The LAMOST stellar classification pipeline uses these empirical templates to identify molecular absorption features (e.g., CaH, TiO; see S. Lépine et al. 2007) and derives the spectral type of an M-dwarf with an accuracy of ± 0.5 subtypes (J. Zhong et al. 2015, 2019). From the LAMOST spectra, TOI-5349 is classified as an $M1 \pm 0.5$ dwarf with $T_e = 3675 \pm 67 \text{ K}$ and $\log g_* = 4.71 \pm 0.07$. The spectroscopic parameters are consistent with the parameters derived from higher-resolution near-infrared spectra in Section 3.1 that are presented in Table 2.

3.3. Fitting the spectral energy distribution

Similar to C. I. Cañas et al. (2023), we derive stellar parameters by modeling the spectral energy distribution (SED) using the EXOFASTv2 analysis package (J. D. Eastman et al. 2019), which fits the observed magnitudes using predictions from the MIST model grids (A. Dotter 2016; J. Choi et al. 2016). The SED fit used Gaussian priors on the (i) broadband photometry listed in Table 2, (ii) spectroscopic parameters from HPF-SpecMatch, and (iii) parallax measurements from Gaia DR3 (Gaia Collaboration et al. 2022). We placed an upper limit on the visual extinction (A_V) based on estimates of Galactic dust (G. M. Green et al. 2019). EXOFASTv2 adopts the $R_v = 3.1$ reddening law from E. L. Fitzpatrick (1999) to calculate a visual magnitude extinction during the SED fit. Table 2 contains the derived stellar parameters. TOI-5349 has a mass and radius of $M_* = 0.61 \pm 0.02 \text{ M}_\odot$ and $R_* = 0.58 \pm 0.02 \text{ R}_\odot$, respectively.

²⁸ <https://www.lamost.org/dr10/v2.0/>

3.4. Galactic kinematics

We calculated the UVW velocities in the barycentric frame using GALPY (J. Bovy 2015) to determine the probabilities of TOI-5349 belonging to the galactic thin disk, thick disk, or halo. Using the equations in T. Bensby et al. (2014), we determine a 98.60% probability that TOI-5349 belongs to the thin-disk population when compared to the halo or thick disk population (see Table 2).

4. DATA ANALYSIS

We performed a joint fit of the RV and photometry data using the `exoplanet` software package (D. Foreman-Mackey et al. 2021), which employs the No-U-Turn Sampler (NUTS) with the Hamiltonian Monte Carlo (HMC) algorithm in PyMC3 (J. Salvatier et al. 2016) for posterior estimation due to its efficiency in exploring the parameter space of correlated, high dimensional posteriors by auto-tuning the step size and choosing the trajectory length via a U-turn criterion. The `exoplanet` package uses `starry` (R. Luger et al. 2019) package to model the photometry data, which applies a quadratic limb-darkening law for transit modeling. The limb-darkening priors were reparameterized following D. M. Kipping (2013) for a quadratic limb-darkening law, with each dataset assigned its own limb-darkening coefficients. The TESS photometry did not exhibit any out-of-transit variability, and we did not include a Gaussian process in our photometric model. The RV data were fitted using a Keplerian model with an eccentric orbit, incorporating an RV offset and a jitter term to account for any systematic differences between instruments and astrophysical factors that may be present. We first obtained the maximum a posteriori (MAP) solution, using random starting conditions from priors specified in Table 3. This MAP solution was then used as the initial conditions for the NUTS sampler. The final joint fit was sampled using 4

independent chains with 6,000 tuning steps and the convergence was assessed using the Gelman-Rubin statistic (all parameters had $\hat{R} < 1.01$; A. Gelman & D. B. Rubin 1992). The system parameters derived from the final joint fit are presented in Table 3. The best-fit transit model is shown in Figure 2, while the best-fit RV model is shown in Figure 3.

5. DISCUSSION

5.1. *TOI-5349b in context of existing GEMS*

We compare TOI-5349b with other well-characterized ($\geq 3\sigma$ mass and radius confidence) GEMS planets and the M-dwarf planet population. Using the NASA Exoplanet Archive (R. L. Akeson et al. 2013), we compiled a sample of GEMS with radii $\gtrsim 8 R_\oplus$, stellar effective temperatures $T_{\text{eff}} < 4000$ K, mass and radius determinations with $\geq 3\sigma$ confidence from the planetary composite table (NASA Exoplanet Science Institute 2020). Figure 6 shows the resulting mass-radius distribution, with density contours overlaid by dashed lines. The GEMS sample ($N = 30$) predominantly falls within a Saturn-like density regime ($0.69 \pm 0.0002 \text{ g cm}^{-3}$), with densities between $0.4 - 0.9 \text{ g cm}^{-3}$ and masses spanning $95 - 140 M_\oplus$. TOI-5349b has a mass of $0.40 \pm 0.02 M_J$ ($127.4_{-5.7}^{+5.9} M_\oplus$) and a radius of $0.91 \pm 0.02 R_J$ ($10.2 \pm 0.03 R_\oplus$), yielding a density of $\rho_p = 0.66 \pm 0.06 \text{ g cm}^{-3}$ making it comparable to other Saturn-density GEMS such as TOI-5344b (J. D. Hartman et al. 2023; T. Han et al. 2024), TOI-5573b (R. B. Fernandes et al. 2025), TOI-5688 Ab (V. Reji et al. 2025), and TOI-6158b (O'Brien et al. in prep.) (See Table 4 for list of properties.)

TOI-5349b falls neatly along the pattern of Saturn-like density GEMS, demonstrating its consistency with other gas giants in this mass regime. Table 4 compares the properties of Saturn-like GEMS (Data from the NASA Exoplanet Archive was queried on 2025 June 20).

Table 3. System parameters for TOI-5349

Parameter	Units	Prior ^a	Value
HPF parameters:			
Systemic velocity	γ (m s ⁻¹)	$\mathcal{N}(0, 2 \times 10^4)$	70 ± 20
RV Jitter	σ_{RV} (m s ⁻¹)	$\mathcal{U}(10^{-3}, 10^3)$	50_{-10}^{+20}
MAROON-X (Blue) parameters:			
Systemic velocity	γ (m s ⁻¹)	$\mathcal{N}(0, 2 \times 10^4)$	19 ± 3
RV Jitter	σ_{RV} (m s ⁻¹)	$\mathcal{U}(10^{-3}, 10^3)$	3_{-2}^{+4}
MAROON-X (Red) parameters:			
Systemic velocity	γ (m s ⁻¹)	$\mathcal{N}(0, 2 \times 10^4)$	19 ± 3
RV Jitter	σ_{RV} (m s ⁻¹)	$\mathcal{U}(10^{-3}, 10^3)$	3_{-2}^{+4}
System parameters:			
Orbital period	P (days)	$\mathcal{N}(3.3, 0.1)$	3.317921 ± 0.000002
Time of mid-transit	T_0 (BJD _{TDB})	$\mathcal{N}(2459521.8, 0.1)$	2459521.8184 ± 0.0005
$\sqrt{e} \cos \omega_*$...	$\mathcal{U}(-1, 1)$	$0.10_{-0.08}^{+0.05}$
$\sqrt{e} \sin \omega_*$...	$\mathcal{U}(-1, 1)$	$-0.13_{-0.09}^{+0.14}$
Scaled radius	R_p/R_*	$\mathcal{U}(0, 1)$	0.161 ± 0.002
Impact parameter	b	$\mathcal{U}(0, 1)$	0.51 ± 0.04
Mass	M_p (M _J)	$\mathcal{U}(10^{-3}, 10^3)$	0.40 ± 0.02
...	M_p (M _⊕)	...	$127.4_{-5.5}^{+5.8}$
Derived parameters:			
Semi-amplitude velocity	K (m s ⁻¹)	...	76.2 ± 2.8
Eccentricity	e	...	$0.03_{-0.02}^{+0.03}, 3\sigma < 0.12$
Argument of periastron	ω_* (degrees)	...	-50_{-20}^{+60}
Scaled semi-major axis	a/R_*	...	13.6 ± 0.3
Orbital inclination	i (degrees)	...	87.9 ± 0.2
Transit duration	T_{14} (hours)	...	$1.95_{-0.05}^{+0.04}$
Radius	R_p (R _J)	...	0.91 ± 0.02
...	R_p (R _⊕)	...	10.2 ± 0.3
Surface gravity	$\log g_p$ (cgs)	...	3.08 ± 0.03
Density	ρ_p (g cm ⁻³)	...	0.66 ± 0.06
Semi-major axis	a (au)	...	0.0369 ± 0.0004
Average Incident flux	$\langle F \rangle$ (S _⊕)	...	44.5 ± 3.7
Equilibrium temperature ^b	T_{eq} (K)	...	719 ± 15

^a $\mathcal{N}(\mu, \sigma)$ is a Gaussian prior with a mean and standard deviation of μ and σ , respectively.
^b $\mathcal{U}(A, B)$ is a uniform prior with lower and upper limits of A and B , respectively.

^bThe planet is assumed to be a blackbody.

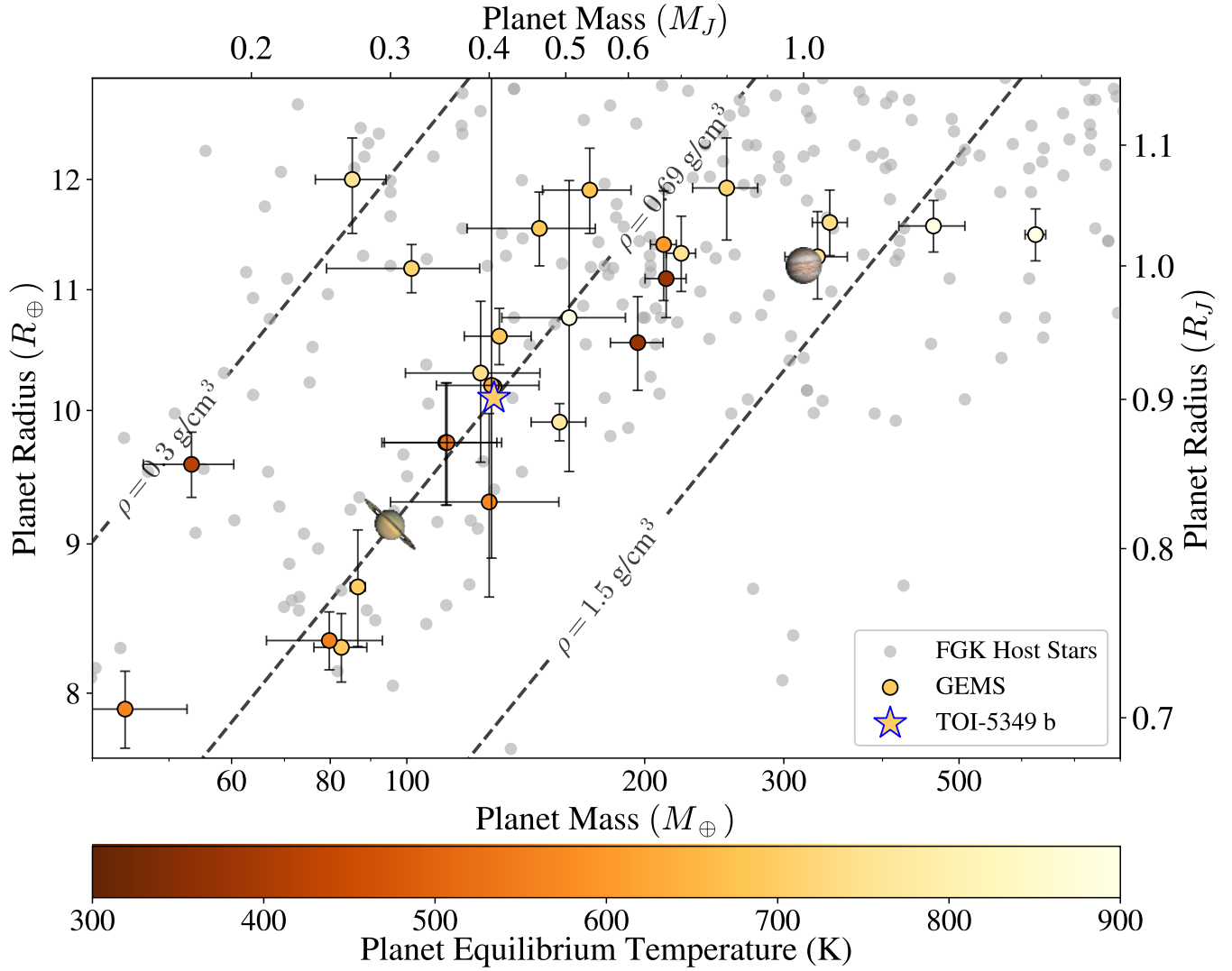


Figure 6. Planet mass as a function of planet radius, highlighting TOI-5349b (denoted by a star symbol) in the context of other GEMS planets. Planet masses are plotted in Earth masses (M_\oplus) and Earth radii (R_\oplus) as well as Jupiter masses (M_J) and Jupiter radii (R_J). TOI-5349b and GEMS targets are color-coded by their planet equilibrium temperature (T_{eq}), with FGK-type host stars shown in gray circles for reference (NASA Exoplanet Science Institute 2020). Density contours corresponding to $\rho = 0.3, 0.69, \text{ and } 1.5 \text{ g cm}^{-3}$ are overlaid as dashed gray lines. Saturn and Jupiter are also shown for comparison. *Uncertainties in mass and radius for TOI-5349b are smaller than the marker size and thus not visible.*

Most exhibit masses of 110–130 M_{\oplus} , radii near $10 R_{\oplus}$, and densities between 0.65 – 0.80 g cm $^{-3}$. Scaled radii ($R_p/R_{\star} \sim 0.16$ –0.22) and separations ($a/R_{\star} \sim 10$ –16) are consistent, suggesting similar environments and potentially disk migration histories with TOI-5349b fitting squarely within these ranges.

Recent work by [S. Kanodia \(2025\)](#) found that when super-Jupiters ($\gtrsim 2 M_{\mathrm{J}}$) are excluded from a sample of transiting giant planets, the average masses of Jupiter-sized planets ($\geq 8 R_{\oplus}$) show no statistical difference between M-dwarfs and FGK hosts. The lack of mass differences suggests that these planets potentially have similar formation processes and initial conditions across different stellar masses, such as a possible minimum disk mass threshold. Metal-rich, high-mass disks appear to be the driving force for forming Saturn- and Jupiter-mass-like planets.

The prevalence of Saturn-like masses and densities among the GEMS population may also be linked to the formation processes involved. The leading theory for the formation of gas giant planets is core accretion ([J. B. Pollack et al. 1996](#); [H. Mizuno 1980](#)), where dust grains in the protoplanetary disk begin clumping to form planetesimals until they reach a $10 M_{\oplus}$ core. After the core reaches this critical mass, it can begin accreting gas and grow into a planet, however, this can also result in forming a range of planetary masses if there is insufficient material for runaway gas accretion. [R. Helled \(2023\)](#) proposed that runaway gas accretion is triggered around Saturn mass or $\sim 100 M_{\oplus}$, marking the transition into gas giant planets. However, this transition is dependent on the exact formation history, stellar environment, and disk gas opacity. The onset of runaway gas accretion can be delayed or impeded through various processes, such as an intermediate phase of heavy-element accretion that can stall or suppress runaway accretion, causing the planet to

remain at a Saturn-like mass if the gas disk disperses early ([A. Vazan et al. 2018](#); [S. Müller et al. 2020](#)). This results in “failed gas giants” which grew large cores but could not accrete the required gas to become Jupiter-mass planets. The similar composition and properties of TOI-5349b and other GEMS planets suggest that these planets may have formed through core-accretion under similar disk conditions where either runaway gas accretion may be limited or there may not be enough heavy element material to form Jupiter-mass objects.

While core accretion remains the favored formation mechanism for gas giants, alternative processes such as gravitational instability ([A. P. Boss 1997, 2006](#)) may be responsible for the formation of some GEMS planets and should not be excluded. In the gravitational instability scenario, regions of a massive, cool protoplanetary disk become unstable and rapidly collapse to form giant planets, bypassing the slow core buildup required by core accretion. Previous studies suggest that gravitational instability may account for the most massive GEMS planets ($\gtrsim 4 M_{\mathrm{J}}$; [R. Helled & P. Bodenheimer 2014](#); [A. Hotnisky et al. 2024](#); [S. Kanodia 2025](#)), such as TOI-2379b ([E. M. Bryant et al. 2024](#)) or TOI-6303b/TOI-6330b ([A. Hotnisky et al. 2024](#)), which show high planet-to-star mass ratios. However, for the Saturn-like GEMS, the more plausible formation pathway appears to be core accretion, possibly quenched before the onset of runaway gas accretion. Additional discoveries and well-characterized systems are still needed to further investigate the formation mechanisms across the GEMS population.

5.2. Metallicity Correlations Among Gas Giants Orbiting M-dwarfs

The GEMS sample shows a strong tendency for orbiting metal-rich stars with the median metallicity of confirmed transiting GEMS hosts being $[\mathrm{Fe}/\mathrm{H}] = +0.27$ dex ([T. Han et al. 2024](#)), significantly higher than that of the typical field

M-dwarf metallicity ($[\text{Fe}/\text{H}] = -0.07$ dex in the H-band and $[\text{Fe}/\text{H}] = +0.07$ dex in the K-band; [T. Gan et al. 2025](#)). This emerging trend mirrors the well-established planet–metallicity correlation observed for hot Jupiters around FGK stars, where giant planets are preferentially found around metal-rich hosts ([G. Gonzalez 1997](#); [D. A. Fischer & J. Valenti 2005](#)).

[T. Gan et al. \(2025\)](#) observed a subset of 22 GEMS and derived metallicities using empirical relationships for spectroscopic observations with SpeX at near-infrared wavelengths ([J. A. Johnson & K. Apps 2009](#); [B. Rojas-Ayala et al. 2010](#); [E. Gaidos et al. 2014](#)) and found that gas giants strongly favor metal-rich M-dwarfs compared to the broader field population. This finding reinforces the notion that metallicity is a significant factor in the formation and evolution of giant planets around low-mass stars. However, future studies using a consistent methodology to derive metallicities may provide more reliable and refined measurements, which may help further refine these correlations. While current metallicity measurements are sufficiently accurate for detailed analyses, it is important to note that they are derived from a combination of spectroscopic and photometric methods, introducing inherent uncertainties. As such, the results should be interpreted with some caution. However, we note that TOI-5349 is confirmed metal-rich by both HPF-SpecMatch and LAMOST spectra, despite the limitations associated with their respective stellar libraries. We therefore adopt the quantitative metallicity

value for TOI-5349 in our analysis while bearing this caveat in mind.

TOI-5349b orbits a metal-rich M1-dwarf star with a metallicity of $[\text{Fe}/\text{H}] = +0.50 \pm 0.16$, confirmed both by HPF-SpecMatch and LAMOST (see [subsection 3.1](#) and [subsection 3.2](#)). This places it among the most metal-rich GEMS hosts to date, second only to HATS-75b ($[\text{Fe}/\text{H}] = +0.52 \pm 0.03$) ([A. Jordán et al. 2022](#)). To place TOI-5349b in context within the broader metallicity trends of GEMS, we plot stellar metallicity as a function of planet density in [Figure 7](#). We observe an emerging trend where low-density gas giants seem to favor higher stellar metallicities, with TOI-5349b aligning neatly with this pattern alongside other Saturn-like GEMS, further supporting this observed correlation.

This pattern among GEMS systems suggests that core accretion is the dominant formation pathway, as high stellar metallicity is strongly correlated with gas giant occurrence. Metal-rich environments improve the solid surface density in protoplanetary disks, thereby accelerating the growth of planetary cores to the critical mass needed to initiate runaway gas accretion before the disk dissipates ([S. Kanodia et al. 2024b](#)). Elevated metallicities increase disk opacity, which can slow radiative cooling during the gas accretion phase. This reduced cooling efficiency may delay or suppress runaway accretion, potentially stalling growth at Saturn-like masses rather than yielding Jupiter analogs ([R. Helled & P. Bodenheimer 2014](#)). This mechanism may help explain why many GEMS planets exhibit masses and radii intermediate between those of Saturn and Jupiter.

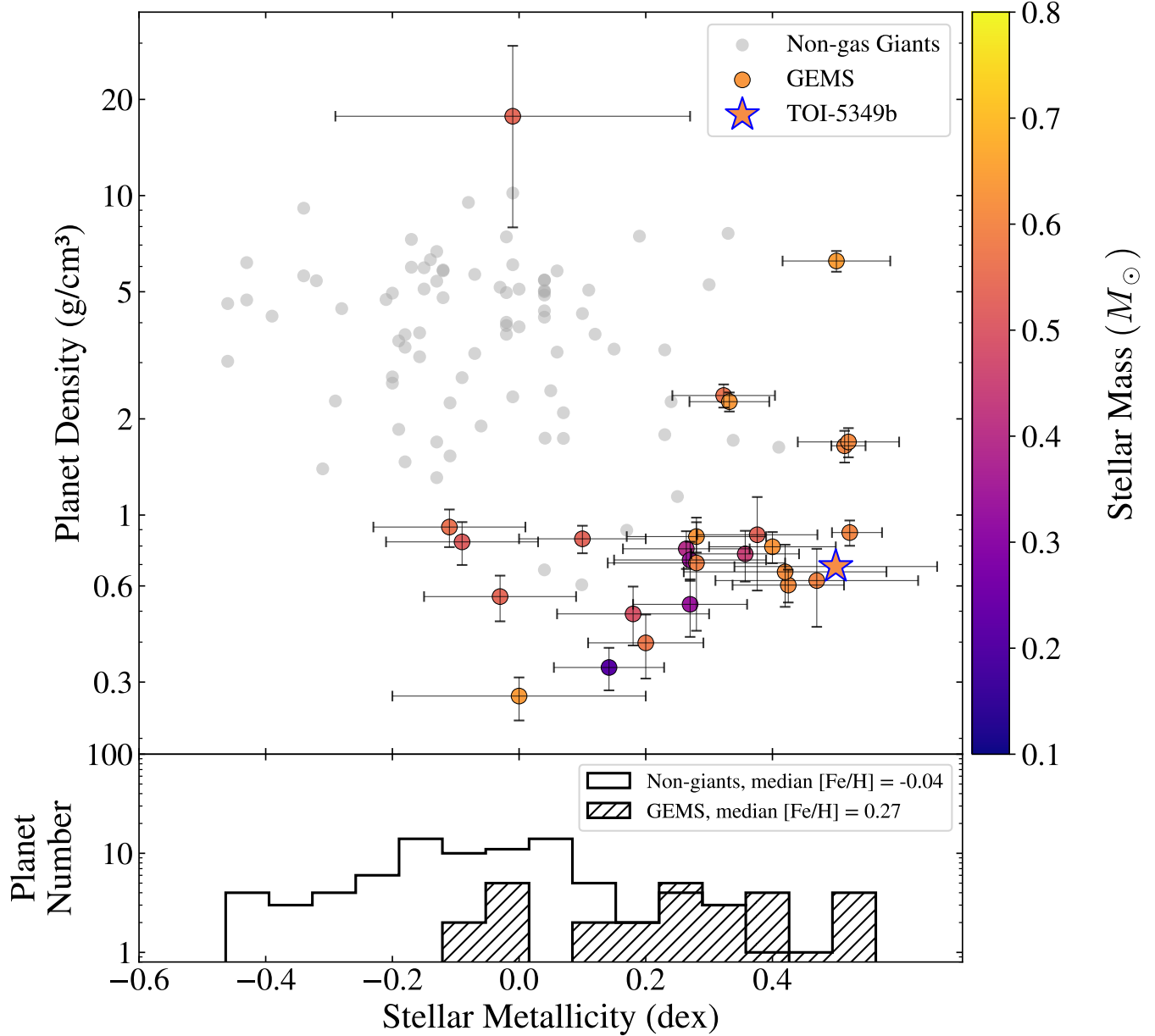


Figure 7. Planet density as a function of stellar metallicity for TOI-5349b (denoted by a star symbol), and other GEMS planets, which are color-coded by their host star mass (M_\star). Non-giant planets (e.g., super-Earths) are plotted in gray for comparison. Densities are plotted on a logarithmic scale in units of g cm^{-3} , and stellar metallicities are given in $[\text{Fe}/\text{H}]$ (dex).

Table 4. Properties of Saturn-like GEMS, sorted by planetary mass.

Planet Name	Orbital Period (days)	Mass (M_\oplus)	Radius (R_\oplus)	T_{eq} (K)	S (S_\oplus)	R_p/R_\star	a/R_\star	Density (g cm^{-3})	Reference
TOI-762 A b	3.47	79.8	8.3	555	17.00	0.18	17.29	0.76	1

Table 4 *continued*

Table 4 (*continued*)

Planet Name	Orbital Period	Mass	Radius	T_{eq}	S	R_p/R_\star	a/R_\star	Density	Reference
	(days)	(M_\oplus)	(R_\oplus)	(K)	(S_\oplus)			(g cm $^{-3}$)	
TOI-3629 b	3.94	82.6	8.3	690	39.00	0.13	15.40	0.80	2, 3
TOI-4860 b	1.52	86.7	8.7	694	42.50	0.22	11.00	0.75	4, 5
TOI-5573 b	8.80	112.0	9.8	528	12.92	0.150	25.74	0.66	6
TOI-5688 A b	2.95	124.0	10.3	742	50.3	0.164	12.5	0.61	7
TOI-6158 b	3.05	128.0	10.2	633	26.7	0.204	15.0	0.65	8
TOI-5349 b	3.32	128.9	10.2	700	44.5	0.161	13.6	0.66	This work
TOI-5344 b	3.79	131.0	10.6	689	38.0	0.1653	14.78	0.60	9, 10
Kepler-45 b	2.46	135.2	10.6	887	85.2	0.153	11.36	0.72	11
HATS-75 b	2.79	156.1	9.9	772	59.26	0.16	12.04	0.88	12

References— 1: J. D. Hartman et al. (2024), 2: C. I. Cañas et al. (2022), 3: J. D. Hartman et al. (2023), 4: A. H. M. J. Triaud et al. (2023), 5: J. M. Almenara et al. (2024), 6: R. B. Fernandes et al. (2025), 7: V. Reji et al. (2025), 8: O'Brien et al. in prep., 9: J. D. Hartman et al. (2023), 10: T. Han et al. (2024), 11: J. A. Johnson et al. (2012) 12: A. Jordán et al. (2022),

5.3. Feasibility of Atmospheric Studies in the GEMS Sample

To further characterize the GEMS population and evaluate their potential for atmospheric observations, we examined the Transmission Spectroscopy Metric (TSM; E. M. R. Kempton et al. 2018) and host star brightness (J-band magnitude). We computed the TSM values for the Saturn-like GEMS sample, incorporating propagated uncertainties from planet radius, mass, stellar radius, equilibrium temperature, and J-band magnitude (see Figure 8).

Across the population, the TSM values span a wide range, from as low as 3.4 to as high as 183.5 ± 12.4 . TOI-5349b has a TSM of 64.0 ± 6.2 , placing it near the median of the current sample. Additionally, TOI-5349b's moderate host star brightness ($J = 12.43$) avoids the saturation limits of JWST NIRSpec PRISM mode ($J \lesssim 11.2$), making it well-suited for complete wavelength coverage observations spanning 0.6 - 5.3 μm without requiring alternative observing methods. Other favorable candidates include TOI-5344b (91.1 ± 12.2), TOI-3629b (79.0 ± 10.5),

and HATS-75b (51.6 ± 5.4), each lying above the typical detectability threshold for transmission spectroscopy. These targets present an opportunity to explore a more diverse set of Saturn-like GEMS orbiting more metal-rich early to mid M-dwarfs.

Atmospheric observations of Saturn-like GEMS, such as TOI-5349b, can offer valuable constraints on formation and evolutionary pathways. These intermediate-mass planets occupy a regime in which atmospheric metallicity (T. Guillot et al. 2023; M. R. Swain et al. 2024), scale height, and cloud structure can diverge significantly from both hot Jupiters and Solar System gas giant planets. Recent transmission spectra of a similar GEMS planet, TOI-5205b, show an incredibly low atmospheric metallicity despite its host star being super-solar in metallicity (S. Kanodia et al. 2023a; C. I. Cañas et al. 2025). The transmission spectra of TOI-5205b reveal that the atmosphere is mainly dominated by stellar contamination from sunspots, along with detections of CH_4 and H_2 highlighting the complex relationship between stellar and planetary composition in these systems. One advan-

tage for studying TOI-5349b is that it orbits a relatively inactive M1 dwarf, which minimizes stellar contamination that can complicate atmospheric retrievals. The TESS photometry and our transit modeling revealed no significant out-of-transit variability and no flares, suggesting limited short-period stellar activity that could complicate atmospheric retrievals. In addition, our spectroscopic diagnostics show no correlation between activity indicators (e.g., differential line width) and the measured RVs. While we cannot fully exclude low-level activity, the absence of strong activity signatures indicates that stellar contamination is unlikely to dominate transmission spectroscopy, making TOI-5349b a favorable target for follow-up atmospheric characterization and could help determine whether the unusual atmospheric properties seen in TOI-5205b represent a broader trend among GEMS planets or reflect unique formation and evolutionary processes.

Moreover, comparative studies of planets with similar bulk properties but differing host star metallicities and effective temperatures are particularly compelling. For instance, TOI-5349b and HATS-75b both orbit metal-rich M-dwarfs and fall within the same Saturn-like regime. HATS-75b is already being targeted under the JWST GO program 3171 (S. Kanodia et al. 2023b), and future observations of TOI-5349b with JWST would be particularly valuable for expanding the sample of Saturn-like GEMS with measured transmission spectra.

6. CONCLUSION

We have presented the discovery and characterization of TOI-5349b, a Saturn-like gas giant ($M_p = 0.40 M_J \approx 127.4^{+5.9}_{-5.7} M_\oplus$, $\rho_p = 0.66 \text{ g cm}^{-3}$) transiting a metal-rich M1 dwarf. With a radius of $0.90 R_J$, TOI-5349b occupies the parameter space of the emerging population of Saturn-like GEMS with radii between $8 - 10 R_\oplus$, masses between $40 - 140 M_\oplus$, and densities typically between $0.4 - 0.9 \text{ g cm}^{-3}$.

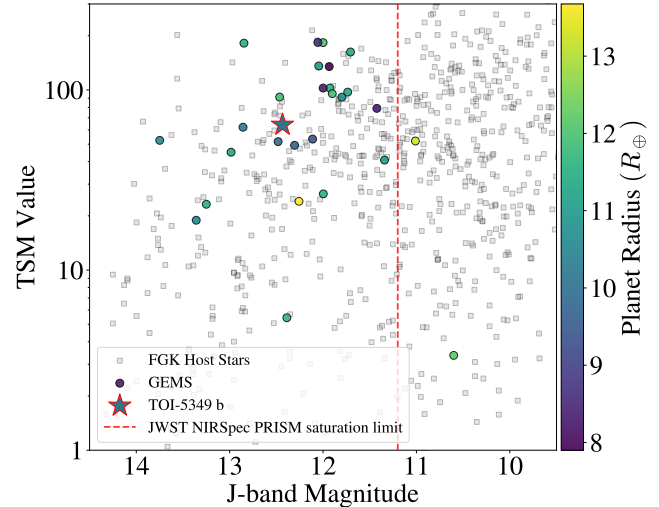


Figure 8. Transmission Spectroscopy Metric (TSM) as a function of host star J-band magnitude for the GEMS sample. The plot highlights how TSM varies with host star J-band magnitude, revealing a steep decline in transmission signal strength for dimmer stars. TOI-5349b lies at $J = 12.43$ with a TSM of 64.0 ± 6.2 , which is well below the saturation threshold for transmission spectroscopy for an early M-dwarf ($J \sim 11.2$; S. M. Birkmann et al. 2022), making it a viable target for observations with JWST.

The super-solar metallicity of the host star and Saturn-like density of the planet support formation through core accretion. TOI-5349b's host star is one of the most metal-rich M-dwarfs known to host a transiting giant, reinforcing the observed trend that GEMS planets form around metal-rich stars. These results add to the increasing evidence that higher dust-to-gas ratios in protoplanetary disks enable the timely formation of massive cores even around lower-mass stars.

In summary, TOI-5349b adds to the emerging picture of Saturn-like planets forming preferentially around metal-rich M-dwarfs, where these planets tend to form in high-metallicity environments and exhibit low densities, supporting core accretion as their dominant formation mechanism. TOI-5349b also reinforces the need to explore how metallicity, stellar mass, and disk

conditions shape the occurrence and properties of gas giants in M-dwarf systems. As the GEMS survey continues to expand this sample, systems like TOI-5349b will serve as key benchmarks for refining planet formation and migration models in low-mass stellar environments.

ACKNOWLEDGMENTS

We thank the anonymous referee for valuable feedback which has improved the quality of this manuscript. AS acknowledges support from the Simons Foundation Presidents Discretionary Fund. CIC acknowledges support from NASA Headquarters through an appointment to the NASA Postdoctoral Program at the Goddard Space Flight Center, administered by ORAU through a contract with NASA. RF acknowledges support from the NASA Hubble Fellowship grant HST-HF2-51559.001-A awarded by the Space Telescope Science Institute, which is operated by the Association of Universities for Research in Astronomy, Inc., for NASA, under contract NAS5-26555.

Resources supporting this work were provided by the (i) NASA High-End Computing Program through the NASA Center for Climate Simulation (NCCS) at Goddard Space Flight Center (ii) Pennsylvania State University's Institute for Computational and Data Sciences' (ICDS) Roar supercomputer, and (iii) VANIR high performance computing cluster at the American Museum of Natural History (AMNH). This content is solely the responsibility of the authors and does not represent the views of NCCS, ICDS, or AMNH.

The Center for Exoplanets and Habitable Worlds is supported by the Pennsylvania State University, the Eberly College of Science, and the Pennsylvania Space Grant Consortium.

We acknowledge support from NSF grants AST 1006676, AST 1126413, AST 1310875, AST 1310885, AST 2009554, AST 2009889, AST 2108512, AST 2108801 and the NASA

Astrobiology Institute (NNA09DA76A) in our pursuit of precision RVs in the near-infrared. We acknowledge the support of the Heising-Simons Foundation through grant 2017-0494. These results are based on observations obtained with HPF on the HET. The HET is a joint project of the University of Texas at Austin, the Pennsylvania State University, Ludwig-Maximilians-Universität München, and Georg-August Universität Gottingen. The HET is named in honor of its principal benefactors, William P. Hobby and Robert E. Eberly. The HET collaboration acknowledges the support and resources from the Texas Advanced Computing Center. We are grateful to the HET Resident Astronomers and Telescope Operators for their valuable assistance in gathering our HPF data. We would like to acknowledge that the HET is built on Indigenous land. Moreover, we would like to acknowledge and pay our respects to the Carrizo & Comecrudo, Coahuiltecan, Caddo, Tonkawa, Comanche, Lipan Apache, Alabama-Coushatta, Kickapoo, Tigua Pueblo, and all the American Indian and Indigenous Peoples and communities who have been or have become a part of these lands and territories in Texas, here on Turtle Island.

Some of the observations in this paper made use of the NN-EXPLORE Exoplanet and Stellar Speckle Imager (NESSI). NESSI was funded by the NASA Exoplanet Exploration Program and the NASA Ames Research Center. NESSI was built at the Ames Research Center by Steve B. Howell, Nic Scott, Elliott P. Horch, and Emmett Quigley.

Some of the observations were obtained using MAROON-X (GN-2023B-Q-104, PI: Kanodia) at the international Gemini Observatory, a program of NSF NOIRLab, which is managed by the Association of Universities for Research in Astronomy (AURA) under a cooperative agreement with the U.S. National Science Foundation on behalf of the Gemini Ob-

servatory partnership: the U.S. National Science Foundation (United States), National Research Council (Canada), Agencia Nacional de Investigación y Desarrollo (Chile), Ministerio de Ciencia, Tecnología e Innovación (Argentina), Ministério da Ciência, Tecnologia, Inovações e Comunicações (Brazil), and Korea Astronomy and Space Science Institute (Republic of Korea). This work was enabled by observations made from the Gemini North telescope, located within the Maunakea Science Reserve and adjacent to the summit of Maunakea. We are grateful for the privilege of observing the Universe from a place that is unique in both its astronomical quality and its cultural significance.

Some of the data presented in this paper were obtained from MAST at STScI. Support for MAST for non-HST data is provided by the NASA Office of Space Science via grant NNX09AF08G and by other grants and contracts. This work includes data collected by the TESS mission, which are publicly available from MAST. Funding for the TESS mission is provided by the NASA Science Mission Directorate. We acknowledge the use of public TOI Release data from pipelines at the TESS Science Office and at the TESS Science Processing Operations Center. This research made use of the (i) NASA Exoplanet Archive, which is operated by Caltech, under contract with NASA under the Exoplanet Exploration Program, (ii) SIMBAD database, operated at CDS, Strasbourg, France, (iii) NASA's Astrophysics Data System Bibliographic Services, (iv) NASA/IPAC Infrared Science Archive, which is funded by NASA and operated by the California Institute of Technology, and (v) data from 2MASS, a joint project of the University of Massachusetts and IPAC at Caltech, funded by NASA and the NSF. The research was carried out, in part, at the Jet Propulsion Laboratory, California Insti-

tute of Technology, under a contract with the National Aeronautics and Space Administration (80NM0018D0004)

This work has used data from the European Space Agency (ESA) mission Gaia (<https://www.cosmos.esa.int/gaia>), processed by the Gaia Data Processing and Analysis Consortium (DPAC, <https://www.cosmos.esa.int/web/gaia/dpac/consortium>). Funding for the DPAC has been provided by national institutions, in particular the institutions participating in the Gaia Multilateral Agreement.

Some of the observations in this paper made use of the Guoshoujing Telescope (LAMOST), a National Major Scientific Project built by the Chinese Academy of Sciences. Funding for the project has been provided by the National Development and Reform Commission. LAMOST is operated and managed by the National Astronomical Observatories, Chinese Academy of Sciences.

Facilities: Exoplanet Archive, Gaia, Gemini:Gillett (MAROON-X), HET (HPF), LAMOST, MAST, RBO, TESS, TMO, WIYN (NESSI)

Software: `astroquery` (A. Ginsburg et al. 2019), `astropy` (Astropy Collaboration et al. 2013, 2018, 2022), `barycorrpy` (S. Kanodia et al. 2018), `EXOFASTv2` (J. D. Eastman et al. 2019), `exoplanet` (D. Foreman-Mackey et al. 2021), `HPF-SERVAL` (G. Stefánsson et al. 2023), `HPF-SpecMatch` (G. Stefánsson et al. 2020), `lightkurve` (Lightkurve Collaboration et al. 2018), `matplotlib` (J. D. Hunter 2007), `numpy` (S. van der Walt et al. 2011), `pandas` (W. McKinney 2010), `PyMC3` (J. Salvatier et al. 2016), `scipy` (P. Virtanen et al. 2020), `starry` (R. Luger et al. 2019), `telfit` (K. Gullikson et al. 2014), `tg1c` (T. Han & T. D. Brandt 2023)

REFERENCES

Akeson, R. L., Chen, X., Ciardi, D., et al. 2013, Publications of the Astronomical Society of the Pacific, 125, 989, doi: [10.1086/672273](https://doi.org/10.1086/672273)

Almenara, J. M., Bonfils, X., Bryant, E. M., et al. 2024, A&A, 683, A166, doi: [10.1051/0004-6361/202346999](https://doi.org/10.1051/0004-6361/202346999)

Astropy Collaboration, Robitaille, T. P., Tollerud, E. J., et al. 2013, *A&A*, 558, A33, doi: [10.1051/0004-6361/201322068](https://doi.org/10.1051/0004-6361/201322068)

Astropy Collaboration, Price-Whelan, A. M., Sipőcz, B. M., et al. 2018, *AJ*, 156, 123, doi: [10.3847/1538-3881/aabc4f](https://doi.org/10.3847/1538-3881/aabc4f)

Astropy Collaboration, Price-Whelan, A. M., Lim, P. L., et al. 2022, *ApJ*, 935, 167, doi: [10.3847/1538-4357/ac7c74](https://doi.org/10.3847/1538-4357/ac7c74)

Bean, J. L., Seifahrt, A., Hartman, H., et al. 2010, *ApJ*, 713, 410, doi: [10.1088/0004-637X/713/1/410](https://doi.org/10.1088/0004-637X/713/1/410)

Bensby, T., Feltzing, S., & Oey, M. S. 2014, *A&A*, 562, A71, doi: [10.1051/0004-6361/201322631](https://doi.org/10.1051/0004-6361/201322631)

Bernabò, L. M., Kanodia, S., Cañas, C. I., et al. 2024, *AJ*, 168, 273, doi: [10.3847/1538-3881/ad7fe8](https://doi.org/10.3847/1538-3881/ad7fe8)

Birkmann, S. M., Ferruit, P., Giardino, G., et al. 2022, *A&A*, 661, A83, doi: [10.1051/0004-6361/202142592](https://doi.org/10.1051/0004-6361/202142592)

Boss, A. P. 1997, *Science*, 276, 1836, doi: [10.1126/science.276.5320.1836](https://doi.org/10.1126/science.276.5320.1836)

Boss, A. P. 2006, *ApJ*, 643, 501, doi: [10.1086/501522](https://doi.org/10.1086/501522)

Boss, A. P., & Kanodia, S. 2023, *ApJ*, 956, 4, doi: [10.3847/1538-4357/acf373](https://doi.org/10.3847/1538-4357/acf373)

Bovy, J. 2015, *ApJS*, 216, 29, doi: [10.1088/0067-0049/216/2/29](https://doi.org/10.1088/0067-0049/216/2/29)

Bryant, E. M., Bayliss, D., Hartman, J. D., et al. 2024, *MNRAS*, 533, 3893, doi: [10.1093/mnras/stae2034](https://doi.org/10.1093/mnras/stae2034)

Cañas, C. I., Kanodia, S., Bender, C. F., et al. 2022, *AJ*, 164, 50, doi: [10.3847/1538-3881/ac7804](https://doi.org/10.3847/1538-3881/ac7804)

Cañas, C. I., Kanodia, S., Libby-Roberts, J., et al. 2023, *AJ*, 166, 30, doi: [10.3847/1538-3881/acdac7](https://doi.org/10.3847/1538-3881/acdac7)

Cañas, C. I., Lustig-Yaeger, J., Tsai, S.-M., et al. 2025, arXiv e-prints, arXiv:2502.06966, doi: [10.48550/arXiv.2502.06966](https://doi.org/10.48550/arXiv.2502.06966)

Chambers, K. C., Magnier, E. A., Metcalfe, N., et al. 2016, arXiv e-prints, arXiv:1612.05560. <https://arxiv.org/abs/1612.05560>

Choi, J., Dotter, A., Conroy, C., et al. 2016, *ApJ*, 823, 102, doi: [10.3847/0004-637X/823/2/102](https://doi.org/10.3847/0004-637X/823/2/102)

Collins, K. A., Kielkopf, J. F., Stassun, K. G., & Hessman, F. V. 2017, *AJ*, 153, 77, doi: [10.3847/1538-3881/153/2/77](https://doi.org/10.3847/1538-3881/153/2/77)

Cui, X.-Q., Zhao, Y.-H., Chu, Y.-Q., et al. 2012, *Research in Astronomy and Astrophysics*, 12, 1197, doi: [10.1088/1674-4527/12/9/003](https://doi.org/10.1088/1674-4527/12/9/003)

Cutri, R. M., Skrutskie, M. F., van Dyk, S., et al. 2003, *VizieR Online Data Catalog*, 2246

Deng, L.-C., Newberg, H. J., Liu, C., et al. 2012, *Research in Astronomy and Astrophysics*, 12, 735, doi: [10.1088/1674-4527/12/7/003](https://doi.org/10.1088/1674-4527/12/7/003)

Dotter, A. 2016, *ApJS*, 222, 8, doi: [10.3847/0067-0049/222/1/8](https://doi.org/10.3847/0067-0049/222/1/8)

Du, B., Luo, A. L., Zhang, S., et al. 2021, *Research in Astronomy and Astrophysics*, 21, 202, doi: [10.1088/1674-4527/21/8/202](https://doi.org/10.1088/1674-4527/21/8/202)

Du, B., Luo, A. L., Wang, S., et al. 2024, *ApJS*, 275, 42, doi: [10.3847/1538-4365/ad85dc](https://doi.org/10.3847/1538-4365/ad85dc)

Eastman, J. D., Rodriguez, J. E., Agol, E., et al. 2019, arXiv e-prints, arXiv:1907.09480. <https://arxiv.org/abs/1907.09480>

El-Badry, K. 2021, Zenodo, doi: [10.5281/zenodo.4435257](https://doi.org/10.5281/zenodo.4435257)

El-Badry, K., Rix, H.-W., & Heintz, T. M. 2021, *MNRAS*, 506, 2269, doi: [10.1093/mnras/stab323](https://doi.org/10.1093/mnras/stab323)

Fernandes, R. B., Kanodia, S., Delamer, M., et al. 2025, arXiv e-prints, arXiv:2505.08947. <https://arxiv.org/abs/2505.08947>

Fischer, D. A., & Valenti, J. 2005, *ApJ*, 622, 1102, doi: [10.1086/428383](https://doi.org/10.1086/428383)

Fitzpatrick, E. L. 1999, *PASP*, 111, 63, doi: [10.1086/316293](https://doi.org/10.1086/316293)

Foreman-Mackey, D., Luger, R., Agol, E., et al. 2021, *The Journal of Open Source Software*, 6, 3285, doi: [10.21105/joss.03285](https://doi.org/10.21105/joss.03285)

Gaia Collaboration, Vallenari, A., Brown, A.G.A., Prusti, T., & et al. 2022, *A&A*, doi: [10.1051/0004-6361/202243940](https://doi.org/10.1051/0004-6361/202243940)

Gaidos, E., Mann, A. W., Lépine, S., et al. 2014, *MNRAS*, 443, 2561, doi: [10.1093/mnras/stu1313](https://doi.org/10.1093/mnras/stu1313)

Gan, T., Theissen, C. A., Wang, S. X., Burgasser, A. J., & Mao, S. 2025, *ApJS*, 276, 47, doi: [10.3847/1538-4365/ad9c65](https://doi.org/10.3847/1538-4365/ad9c65)

Gelman, A., & Rubin, D. B. 1992, *Statistical Science*, 7, 457, doi: [10.1214/ss/1177011136](https://doi.org/10.1214/ss/1177011136)

Ginsburg, A., Sipőcz, B. M., Brasseur, C. E., et al. 2019, *AJ*, 157, 98, doi: [10.3847/1538-3881/aafc33](https://doi.org/10.3847/1538-3881/aafc33)

Gonzalez, G. 1997, *MNRAS*, 285, 403, doi: [10.1093/mnras/285.2.403](https://doi.org/10.1093/mnras/285.2.403)

Green, G. M., Schlafly, E., Zucker, C., Speagle, J. S., & Finkbeiner, D. 2019, *ApJ*, 887, 93, doi: [10.3847/1538-4357/ab5362](https://doi.org/10.3847/1538-4357/ab5362)

Guerrero, N. M., Seager, S., Huang, C. X., et al. 2021, *ApJS*, 254, 39, doi: [10.3847/1538-4365/abefe1](https://doi.org/10.3847/1538-4365/abefe1)

Guillot, T., Fletcher, L. N., Helled, R., et al. 2023, in *Astronomical Society of the Pacific Conference Series*, Vol. 534, *Protostars and Planets VII*, ed. S. Inutsuka, Y. Aikawa, T. Muto, K. Tomida, & M. Tamura, 947, doi: [10.48550/arXiv.2205.04100](https://doi.org/10.48550/arXiv.2205.04100)

Gullikson, K., Dodson-Robinson, S., & Kraus, A. 2014, *AJ*, 148, 53, doi: [10.1088/0004-6256/148/3/53](https://doi.org/10.1088/0004-6256/148/3/53)

Han, T., & Brandt, T. D. 2023, *AJ*, 165, 71, doi: [10.3847/1538-3881/acaaa7](https://doi.org/10.3847/1538-3881/acaaa7)

Han, T., Robertson, P., Kanodia, S., et al. 2024, *AJ*, 167, 4, doi: [10.3847/1538-3881/ad09c2](https://doi.org/10.3847/1538-3881/ad09c2)

Hartman, J. D., Bakos, G. Á., Csabry, Z., et al. 2023, *AJ*, 166, 163, doi: [10.3847/1538-3881/acf56e](https://doi.org/10.3847/1538-3881/acf56e)

Hartman, J. D., Bayliss, D., Brahm, R., et al. 2024, *AJ*, 168, 202, doi: [10.3847/1538-3881/ad6f07](https://doi.org/10.3847/1538-3881/ad6f07)

Helled, R. 2023, *A&A*, 675, L8, doi: [10.1051/0004-6361/202346850](https://doi.org/10.1051/0004-6361/202346850)

Helled, R., & Bodenheimer, P. 2014, *ApJ*, 789, 69, doi: [10.1088/0004-637X/789/1/69](https://doi.org/10.1088/0004-637X/789/1/69)

Hill, G. J., Lee, H., MacQueen, P. J., et al. 2021, *AJ*, 162, 298, doi: [10.3847/1538-3881/ac2c02](https://doi.org/10.3847/1538-3881/ac2c02)

Hobson, M. J., Jordán, A., Bryant, E. M., et al. 2023, *ApJL*, 946, L4, doi: [10.3847/2041-8213/acbd9a](https://doi.org/10.3847/2041-8213/acbd9a)

Hotnisky, A., Kanodia, S., Libby-Roberts, J., et al. 2024, arXiv e-prints, arXiv:2411.08159, doi: [10.48550/arXiv.2411.08159](https://doi.org/10.48550/arXiv.2411.08159)

Howell, S. B., Everett, M. E., Sherry, W., Horch, E., & Ciardi, D. R. 2011, *AJ*, 142, 19, doi: [10.1088/0004-6256/142/1/19](https://doi.org/10.1088/0004-6256/142/1/19)

Hunter, J. D. 2007, *Computing In Science & Engineering*, 9, 90, doi: [10.1109/MCSE.2007.55](https://doi.org/10.1109/MCSE.2007.55)

Johnson, J. A., & Apps, K. 2009, *ApJ*, 699, 933, doi: [10.1088/0004-637X/699/2/933](https://doi.org/10.1088/0004-637X/699/2/933)

Johnson, J. A., Gazak, J. Z., Apps, K., et al. 2012, *AJ*, 143, 111, doi: [10.1088/0004-6256/143/5/111](https://doi.org/10.1088/0004-6256/143/5/111)

Jordán, A., Hartman, J. D., Bayliss, D., et al. 2022, *AJ*, 163, 125, doi: [10.3847/1538-3881/ac4a77](https://doi.org/10.3847/1538-3881/ac4a77)

Kanodia, S. 2025, *ApJ*, 978, 97, doi: [10.3847/1538-4357/ad9823](https://doi.org/10.3847/1538-4357/ad9823)

Kanodia, S., & Wright, J. 2018, *Research Notes of the American Astronomical Society*, 2, 4, doi: [10.3847/2515-5172/aaa4b7](https://doi.org/10.3847/2515-5172/aaa4b7)

Kanodia, S., Mahadevan, S., Ramsey, L. W., et al. 2018, in *Society of Photo-Optical Instrumentation Engineers (SPIE) Conference Series*, Vol. 10702, *Ground-based and Airborne Instrumentation for Astronomy VII*, ed. C. J. Evans, L. Simard, & H. Takami, 107026Q, doi: [10.1117/12.2313491](https://doi.org/10.1117/12.2313491)

Kanodia, S., Mahadevan, S., Libby-Roberts, J., et al. 2023a, *AJ*, 165, 120, doi: [10.3847/1538-3881/acabce](https://doi.org/10.3847/1538-3881/acabce)

Kanodia, S., Canas, C., Libby-Roberts, J., et al. 2023b, *JWST Proposal. Cycle 2*, ID. #3171

Kanodia, S., Gupta, A. F., Cañas, C. I., et al. 2024a, *AJ*, 168, 235, doi: [10.3847/1538-3881/ad7796](https://doi.org/10.3847/1538-3881/ad7796)

Kanodia, S., Cañas, C. I., Mahadevan, S., et al. 2024b, *AJ*, 167, 161, doi: [10.3847/1538-3881/ad27cb](https://doi.org/10.3847/1538-3881/ad27cb)

Kasper, D. H., Ellis, T. G., Yeigh, R. R., et al. 2016, *PASP*, 128, 105005, doi: [10.1088/1538-3873/128/968/105005](https://doi.org/10.1088/1538-3873/128/968/105005)

Kempton, E. M. R., Bean, J. L., Louie, D. R., et al. 2018, *PASP*, 130, 114401, doi: [10.1088/1538-3873/aadf6f](https://doi.org/10.1088/1538-3873/aadf6f)

Kipping, D. M. 2013, *MNRAS*, 435, 2152, doi: [10.1093/mnras/stt1435](https://doi.org/10.1093/mnras/stt1435)

Kipping, D. M. 2014, *MNRAS*, 440, 2164, doi: [10.1093/mnras/stu318](https://doi.org/10.1093/mnras/stu318)

Kunimoto, M., Daylan, T., Guerrero, N., et al. 2022, *ApJS*, 259, 33, doi: [10.3847/1538-4365/ac5688](https://doi.org/10.3847/1538-4365/ac5688)

Laughlin, G., Bodenheimer, P., & Adams, F. C. 2004, *ApJL*, 612, L73, doi: [10.1086/424384](https://doi.org/10.1086/424384)

Lépine, S., Rich, R. M., & Shara, M. M. 2007, *ApJ*, 669, 1235, doi: [10.1086/521614](https://doi.org/10.1086/521614)

Lightkurve Collaboration, Cardoso, J. V. d. M. a., Hedges, C., et al. 2018, <http://ascl.net/1812.013>

Lin, D. N. C., Bodenheimer, P., & Richardson, D. C. 1996, *Nature*, 380, 606, doi: [10.1038/380606a0](https://doi.org/10.1038/380606a0)

Luger, R., Agol, E., Foreman-Mackey, D., et al. 2019, *AJ*, 157, 64, doi: [10.3847/1538-3881/aae8e5](https://doi.org/10.3847/1538-3881/aae8e5)

Mahadevan, S., Ramsey, L., Bender, C., et al. 2012, in Society of Photo-Optical Instrumentation Engineers (SPIE) Conference Series, Vol. 8446, Ground-based and Airborne Instrumentation for Astronomy IV, ed. I. S. McLean, S. K. Ramsay, & H. Takami, 84461S, doi: [10.1117/12.926102](https://doi.org/10.1117/12.926102)

Mahadevan, S., Ramsey, L. W., Terrien, R., et al. 2014, in Society of Photo-Optical Instrumentation Engineers (SPIE) Conference Series, Vol. 9147, Ground-based and Airborne Instrumentation for Astronomy V, ed. S. K. Ramsay, I. S. McLean, & H. Takami, 91471G, doi: [10.1117/12.2056417](https://doi.org/10.1117/12.2056417)

McKinney, W. 2010, in Proceedings of the 9th Python in Science Conference, ed. S. van der Walt & J. Millman, 51 – 56

Mizuno, H. 1980, Progress of Theoretical Physics, 64, 544, doi: [10.1143/PTP.64.544](https://doi.org/10.1143/PTP.64.544)

Müller, S., Ben-Yami, M., & Helled, R. 2020, ApJ, 903, 147, doi: [10.3847/1538-4357/abba19](https://doi.org/10.3847/1538-4357/abba19)

NASA Exoplanet Science Institute. 2020,, NASA IPAC DataSet, NEA13 doi: [10.26133/NEA13](https://doi.org/10.26133/NEA13)

Ninan, J. P., Bender, C. F., Mahadevan, S., et al. 2018, in Society of Photo-Optical Instrumentation Engineers (SPIE) Conference Series, Vol. 10709, High Energy, Optical, and Infrared Detectors for Astronomy VIII, ed. A. D. Holland & J. Beletic, 107092U, doi: [10.1117/12.2312787](https://doi.org/10.1117/12.2312787)

Pollack, J. B., Hubickyj, O., Bodenheimer, P., et al. 1996, Icarus, 124, 62, doi: [10.1006/icar.1996.0190](https://doi.org/10.1006/icar.1996.0190)

Ramsey, L. W., Adams, M. T., Barnes, T. G., et al. 1998, in Society of Photo-Optical Instrumentation Engineers (SPIE) Conference Series, Vol. 3352, Advanced Technology Optical/IR Telescopes VI, ed. L. M. Stepp, 34–42, doi: [10.1117/12.319287](https://doi.org/10.1117/12.319287)

Reji, V., Kanodia, S., Ninan, J. P., et al. 2025, AJ, 169, 187, doi: [10.3847/1538-3881/ada7ea](https://doi.org/10.3847/1538-3881/ada7ea)

Ricker, G. R., Winn, J. N., Vanderspek, R., et al. 2015, Journal of Astronomical Telescopes, Instruments, and Systems, 1, 014003, doi: [10.1117/1.JATIS.1.1.014003](https://doi.org/10.1117/1.JATIS.1.1.014003)

Rojas-Ayala, B., Covey, K. R., Muirhead, P. S., & Lloyd, J. P. 2010, ApJL, 720, L113, doi: [10.1088/2041-8205/720/1/L113](https://doi.org/10.1088/2041-8205/720/1/L113)

Salvatier, J., Wiecki, T. V., & Fonnesbeck, C. 2016,, Astrophysics Source Code Library, record ascl:1610.016

Schönrich, R., Binney, J., & Dehnen, W. 2010, MNRAS, 403, 1829, doi: [10.1111/j.1365-2966.2010.16253.x](https://doi.org/10.1111/j.1365-2966.2010.16253.x)

Scott, N. J., Howell, S. B., Horch, E. P., & Everett, M. E. 2018, PASP, 130, 054502, doi: [10.1088/1538-3873/aab484](https://doi.org/10.1088/1538-3873/aab484)

Seager, S., & Mallén-Ornelas, G. 2003, ApJ, 585, 1038, doi: [10.1086/346105](https://doi.org/10.1086/346105)

Seifahrt, A., Bean, J. L., Stürmer, J., et al. 2016, in Society of Photo-Optical Instrumentation Engineers (SPIE) Conference Series, Vol. 9908, Ground-based and Airborne Instrumentation for Astronomy VI, ed. C. J. Evans, L. Simard, & H. Takami, 990818, doi: [10.1117/12.2232069](https://doi.org/10.1117/12.2232069)

Seifahrt, A., Stürmer, J., Bean, J. L., & Schwab, C. 2018, in Society of Photo-Optical Instrumentation Engineers (SPIE) Conference Series, Vol. 10702, Ground-based and Airborne Instrumentation for Astronomy VII, ed. C. J. Evans, L. Simard, & H. Takami, 107026D, doi: [10.1117/12.2312936](https://doi.org/10.1117/12.2312936)

Seifahrt, A., Bean, J. L., Stürmer, J., et al. 2020, in Society of Photo-Optical Instrumentation Engineers (SPIE) Conference Series, Vol. 11447, Ground-based and Airborne Instrumentation for Astronomy VIII, ed. C. J. Evans, J. J. Bryant, & K. Motohara, 114471F, doi: [10.1117/12.2561564](https://doi.org/10.1117/12.2561564)

Seifahrt, A., Bean, J. L., Kasper, D., et al. 2022, in Society of Photo-Optical Instrumentation Engineers (SPIE) Conference Series, Vol. 12184, Ground-based and Airborne Instrumentation for Astronomy IX, ed. C. J. Evans, J. J. Bryant, & K. Motohara, 121841G, doi: [10.1117/12.2629428](https://doi.org/10.1117/12.2629428)

Shetrone, M., Cornell, M. E., Fowler, J. R., et al. 2007, PASP, 119, 556, doi: [10.1086/519291](https://doi.org/10.1086/519291)

Stassun, K. G., Oelkers, R. J., Paegert, M., et al. 2019, AJ, 158, 138, doi: [10.3847/1538-3881/ab3467](https://doi.org/10.3847/1538-3881/ab3467)

Stefansson, G., Hearty, F., Robertson, P., et al. 2016, ApJ, 833, 175, doi: [10.3847/1538-4357/833/2/175](https://doi.org/10.3847/1538-4357/833/2/175)

Stefánsson, G., Cañas, C., Wisniewski, J., et al. 2020, AJ, 159, 100, doi: [10.3847/1538-3881/ab5f15](https://doi.org/10.3847/1538-3881/ab5f15)

Stefánsson, G., Mahadevan, S., Miguel, Y., et al. 2023, *Science*, 382, 1031, doi: [10.1126/science.abo0233](https://doi.org/10.1126/science.abo0233)

Swain, M. R., Hasegawa, Y., Thorngren, D. P., & Roudier, G. M. 2024, *SSRv*, 220, 61, doi: [10.1007/s11214-024-01098-7](https://doi.org/10.1007/s11214-024-01098-7)

Triaud, A. H. M. J., Dransfield, G., Kagetani, T., et al. 2023, *MNRAS*, 525, L98, doi: [10.1093/mnrasl/slad097](https://doi.org/10.1093/mnrasl/slad097)

van der Walt, S., Colbert, S. C., & Varoquaux, G. 2011, *Computing in Science and Engineering*, 13, 22, doi: [10.1109/MCSE.2011.37](https://doi.org/10.1109/MCSE.2011.37)

Vazan, A., Ormel, C. W., Noack, L., & Dominik, C. 2018, *ApJ*, 869, 163, doi: [10.3847/1538-4357/aaef33](https://doi.org/10.3847/1538-4357/aaef33)

Virtanen, P., Gommers, R., Oliphant, T. E., et al. 2020, *Nature Methods*, 17, 261, doi: [10.1038/s41592-019-0686-2](https://doi.org/10.1038/s41592-019-0686-2)

Wang, X.-Y., Rice, M., Wang, S., et al. 2022, *ApJL*, 926, L8, doi: [10.3847/2041-8213/ac4f44](https://doi.org/10.3847/2041-8213/ac4f44)

Winn, J. N. 2010, in *Exoplanets*, ed. S. Seager, 55–77, doi: [10.48550/arXiv.1001.2010](https://doi.org/10.48550/arXiv.1001.2010)

Wright, E. L., Eisenhardt, P. R. M., Mainzer, A. K., et al. 2010, *AJ*, 140, 1868, doi: [10.1088/0004-6256/140/6/1868](https://doi.org/10.1088/0004-6256/140/6/1868)

Wright, J. T., & Eastman, J. D. 2014, *PASP*, 126, 838, doi: [10.1086/678541](https://doi.org/10.1086/678541)

Xiang, M. S., Liu, X. W., Yuan, H. B., et al. 2017, *MNRAS*, 467, 1890, doi: [10.1093/mnras/stx129](https://doi.org/10.1093/mnras/stx129)

Yee, S. W., Petigura, E. A., & von Braun, K. 2017, *ApJ*, 836, 77, doi: [10.3847/1538-4357/836/1/77](https://doi.org/10.3847/1538-4357/836/1/77)

Yuan, H. B., Liu, X. W., Huo, Z. Y., et al. 2015, *MNRAS*, 448, 855, doi: [10.1093/mnras/stu2723](https://doi.org/10.1093/mnras/stu2723)

Zechmeister, M., Reiners, A., Amado, P. J., et al. 2018, *A&A*, 609, A12, doi: [10.1051/0004-6361/201731483](https://doi.org/10.1051/0004-6361/201731483)

Zhong, J., Li, J., Carlin, J. L., et al. 2019, *ApJS*, 244, 8, doi: [10.3847/1538-4365/ab3859](https://doi.org/10.3847/1538-4365/ab3859)

Zhong, J., Lépine, S., Hou, J., et al. 2015, *AJ*, 150, 42, doi: [10.1088/0004-6256/150/2/42](https://doi.org/10.1088/0004-6256/150/2/42)